frontiers | Frontiers in Earth Science

TYPE Original Research
PUBLISHED 30 July 2024
DOI 10.3389/feart.2024.1431866

OPEN ACCESS

EDITED BY
Lawrence H. Tanner,
Le Moyne College, United States

REVIEWED BY
Gaoxue Yang,
Chang'an University, China
Su-Chin Chang,
The University of Hong Kong, Hong Kong SAR, China

*CORRESPONDENCE
Lin Jiang,
jianglin01@petrochina.com.cn

RECEIVED 13 May 2024
ACCEPTED 28 June 2024
PUBLISHED 30 July 2024

CITATION
Gao Y, Jiang L, Chen W, Jiang F, Dong H, Zhao W, Dong C and Feng Y (2024), Provenance of cretaceous sediments in the West Kunlun piedmont belt and implications for tectonic evolutionary events.
Front. Earth Sci. 12:1431866.
doi: 10.3389/feart.2024.1431866

Provenance of cretaceous sediments in the West Kunlun piedmont belt and implications for tectonic evolutionary events

Yang Gao[1,2,3,4], Lin Jiang[1,3,4]*, Weiyan Chen[3,4], Fujie Jiang[1,2], Hongkui Dong[3], Wen Zhao[3], Changyu Dong[1,2] and Yingqi Feng[5]

[1]National Key Laboratory of Petroleum Resources and Engineering, China University of Petroleum, Beijing, China, [2]College of Geosciences, China University of Petroleum, Beijing, China, [3]Research Institute of Petroleum Exploration and Development, PetroChina, Beijing, China, [4]CNPC Key Laboratory of Basin Structure and Hydrocarbon Accumulation, Beijing, China, [5]School of Geosciences, China University of Petroleum (East China), Qingdao, China

The West Kunlun orogenic belt located in the northwestern margin of the Qinghai-Tibet Plateau is an important record of the formation and northward extension of the plateau, but the current research mainly focuses on the tectonic activities of the Cenozoic era, and there is still considerable controversy regarding the formation and evolutionary history of pre-Cenozoic orogenic belts. This study focuses on Cretaceous sandstone samples from the Kedong region in the piedmont belt of the West Kunlun orogenic belt. U-Pb geochronological analysis was performed on 200 detrital zircon grains from the core samples. Combined with stratigraphic data and previous research, the main provenance direction was investigated to constrain the tectonic evolutionary history of the orogenic belt's peripheral regions. The results show that the detrital zircons are aged from 290 to 208 Ma, 520–310 Ma, 810–580 Ma, 1,400–880 Ma and 2,548–1,730 Ma, reflecting the complexity of provenance in this area. Based on a comprehensive analysis of the characteristics of igneous rocks, zircon age composition and stratigraphic conditions in potential source areas, it is concluded that the primary source regions include the East Kunlun orogenic belt and the North and South Kunlun terranes, with a low likelihood of contributions from within the Tarim Basin. The evolution of the West Kunlun orogenic belt can generally be divided into two opening and two closing phases. The detrital zircon ages predominantly exhibit two peak values at 259 Ma and 459 Ma, respectively representing the ages of transition from oceanic crust subduction to continent-continent collision for the Paleo-Tethys Ocean and the Proto-Tethys Ocean. Additionally, there is a temporal gap between the evolution of the Proto-Tethys Ocean and the Paleo-Tethys Ocean. The Triassic period marks a transitional phase in tectonic evolution, shifting into an intracontinental evolutionary stage. This study provides new geochronological evidence for the early developmental history of the West Kunlun orogenic belt.

KEYWORDS

West Kunlun orogen belt, detrital zircon U-Pb geochronology, provenance, TETHYS, mountaian building

1 Introduction

The West Kunlun orogenic belt is located in the northwest margin of the Qinghai-Tibet Plateau, bordering the Tarim Basin to the north, the Qiangtang Terrane to the south, the Pamir Plateau to the west, and the Altun Fault zone to the east (Figure 1A). Compared with other orogenic belts, the West Kunlun orogenic belt has two special features: First, the West Kunlun orogenic belt was formed by the combination of multiple terranes from Paleozoic to Mesozoic, and these terranes are separated by deep faults nowadays; Second, the piedmont belt where the Western Kunlun orogenic belt intersects with the southwestern Tarim Basin has developed the longest foreland fold-and-thrust belt in western China, extending approximately 230 km and accumulating nearly ten thousand meters of clastic sediments. The piedmont belt refers to the transition zone between the orogenic belt and the sedimentary basin, which is the most active and frequent region in the continental interior, and is also one of the important windows to understand the history of plate convergence and surface evolution of the earth. Therefore, the West Kunlun piedmont belt is an ideal region to understand the formation process of the West Kunlun orogenic belt and the tectonic evolution of the northern margin of the Qinghai-Tibet Plateau (John et al., 2012; Guo et al., 2013; Cao et al., 2015; Blayney et al., 2016; Wu et al., 2021). The tectonic evolution of the West Kunlun orogenic belt has been studied by petrology, geochemistry and detrital zircon chronology. Zhang et al. (2016) found a large number of 500–200 Ma granites associated with ocean basin subduction and closure orogeny in the West Kunlun area, suggesting that the formation of the West Kunlun area is directly related to the evolution of the Tethys Ocean (Zhang et al., 2016); Based on zircon dating of gneiss exposed from the Mazar-Kangxiwar fault and early geological data, Yang et al. (2010) suggest that the Mesozoic collision orogeny of the West Kunlun orogenic belt occurred in the Middle to Late Triassic (Yang et al., 2010); According to the comprehensive study and analysis of different granites in the north of West Kunlun by Zhang et al. (2005), the Mesozoic collisional orogeny of the West Kunlun orogenic belt occurred in the Late Permian-Middle Triassic period (Zhang et al., 2005). On the whole, the current tectonic research related to the West Kunlun has the following deficiencies: 1) The tectonic activities of the southwest margin of Tarim and the West Kunlun orogenic belt are mainly focused on the analysis of granite and suture zone, while granite is generally developed in the stages of continental cracking and ocean crust subduction, and its interpretation has a single direction of activity and multiple solutions of different activities; 2) In previous studies, sedimentary rocks from typical outcrops were selected, and there was unity, ignoring the huge thick sediments in the piedmont zone that recorded the co-evolution of the two regions; 3) Previous studies mainly discussed the matching relationship of tectonothermal events based on the age of detrital zircons in general, and lacked detailed comparison with potential source areas As a result of these factors, the understanding of the tectonic evolution of the southwest Tarim and West Kunlun orogenic belt is still controversial and needs to be further studied.

The piedmont area has great potential for oil and gas resources and low exploration degree. Two important oil and gas fields, Kekeya and Akemomu, have been discovered in recent years, which is the next key area for oil and gas exploration in Tarim. However, at present, the current understanding of the structures and faults in the piedmont belt gas reservoirs of southwestern Tarim is limited, and predictions regarding high-quality reservoirs and hydrocarbon-rich areas are inaccurate. This has resulted in multiple drilling failures in recent years. One of the important factors is that the control factors of sedimentation and filling are not clear, which leads to insufficient understanding of sedimentary reservoirs. Therefore, understanding the provenance of the piedmont belt has two important meanings: one is to predict the long-term tectonic coupling between the evolution of the West Kunlun orogenic belt and the Tarim Basin, the other is to better understand the macro-control factors of sedimentary reservoir distribution, which provides some new ideas for oil and gas exploration in the piedmont area. The sediment provenance of the Cretaceous strata in focus in this paper has been studied by predecessors. Zhang et al. (2021) through provenance analysis of the Cretaceous strata in the typical outcrops section under the West Kunlun orogenic belt, concluded that the granite belt in the West Kunlun area is the provenance of the southwest margin of the Tarim Basin in the Cretaceous period (Zhang et al., 2021). Through outcrop, drilling correlation and heavy mineral analysis, Zhang et al. (2014) believe that the provenance of the early Cretaceous in the piedmonda came from the South Tianshan and West Kunlun orogenic belt (Zhang et al., 2014). In general, previous studies have the above problems (2) and (3), leading to controversial research results. Detrital zircon U-Pb dating technique is a method to determine the formation age of detrital zircon grains by analyzing the U-Pb isotope ratio of detrital zircons in sedimentary rocks. Because of its ability to provide critical information about sediment provenance and their sedimentary ages, this technique has been used in recent years to determine provenance, reconstruct paleogeography, and recover tectonic evolution (Zhu et al., 2011; Cawood et al., 2012). This paper focuses on the thick sediments in the West Kunlun orogenic belt, and on the basis of fine chronology analysis of detrital zircon U-Pb dating, analyzes the provenance characteristics of different terranes to the West Kunlun orogenic belt, and further discusses and defines the co-evolution of the southwest margin of Tarim and the West Kunlun orogenic belt in different periods.

2 Geological settings

The West Kunlun orogenic belt, located at the junction of the Tarim Craton and the Qinghai-Tibet Plateau, represents the product of the subduction of the Paleo-Tethys and Proto-Tethys oceans and the proliferation of continental and marine debris from the Early Paleozoic to Early Mesozoic periods (Zhang et al., 2017). Three main fault zones developed in the orogenic belt, namely, the Kudi suture zone, Kangxiwar fault and Hongshanhu fault from north to south, and these faults as boundaries, the orogenic belt from north to south can be divided into three tectonic terranes, namely, the North Kunlun terrane, the South Kunlun terrane and the Tianshuihai terrane (Figure 1B). The common point of the three terranes is that they all developed Precambrian basement. The North Kunlun terrane is considered to be the front part of the uplift of the southwestern Tarim Craton. The sedimentary strata are Devonian grinding conglomerate, carboniferous and Permian shallow Marine carbonate rocks and post-Permian continental sedimentary rocks

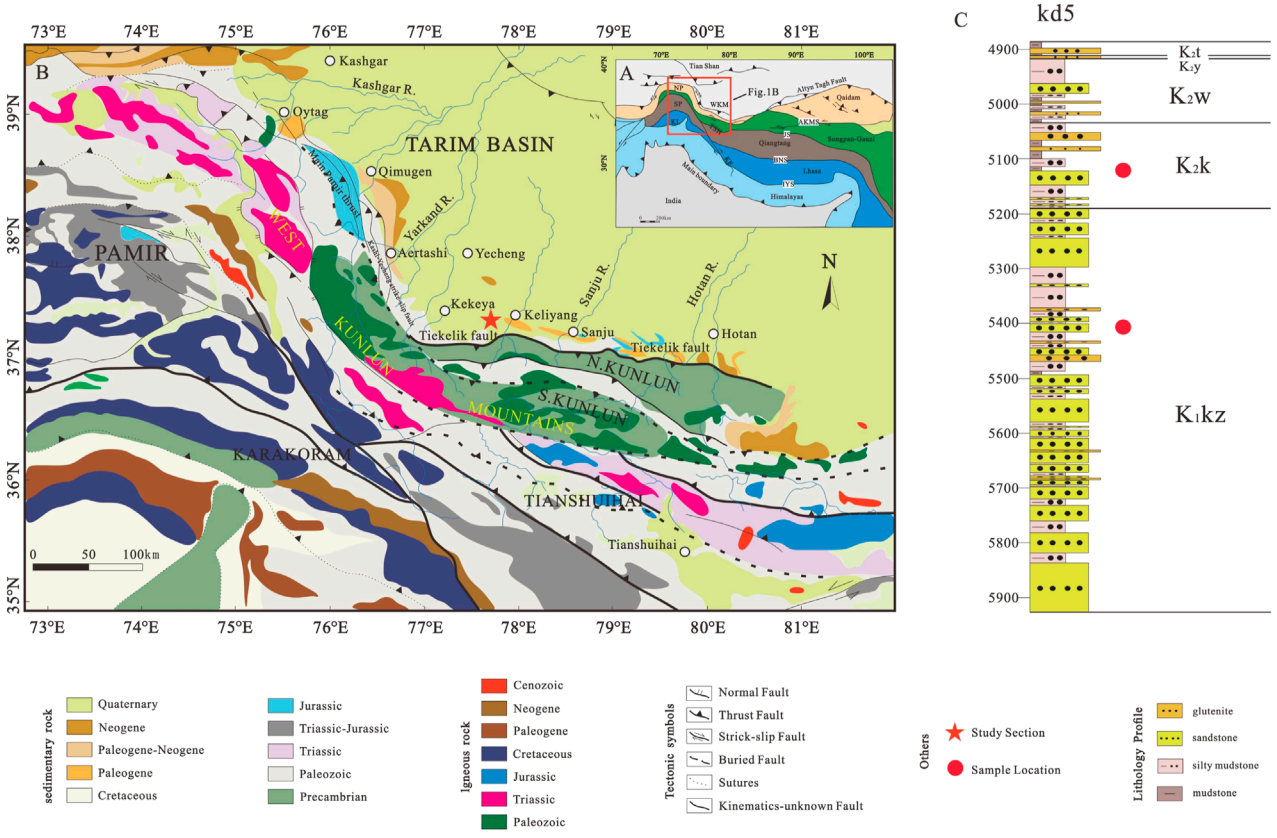

FIGURE 1
(A) Geological map of the west Kunlun orogenic belt. **(B)** Simplified tectonic map of Pamir-Tibetan orogen (modified after Cao et al., 2015). (1) Kudi suture; (2) Kangxiwar suture; (3) Hongshanhu suture. **(C)** Lithologic column map and label of sampling horizon in West Kunlun piedmont zone. K_2t, tuyiluoke; K_2y, yigeziya; K_2w, wuyitake; K_2k, kukebai; K_1kz, kezilesu.

(Yin et al., 2020). The South Kunlun terrane is considered to be an independent external terrane. The sedimentary strata are siliceous rocks, carbonate rocks and calc-alkaline igneous rocks from Upper Paleozoic to Mesozoic (Yuan et al., 2002). The Tianshuihai terrane is considered to be a huge accretionary wedge or independent external terrane related to orogeny. The sedimentary strata are Paleozoic carbonate rocks, Mesozoic pyroclastic materials and continental sedimentary rocks (Hu et al., 2016).

Under the influence of the continuous collision and convergence between the Indian plate and the Eurasian plate since Cenozoic, the Tiekelik fault develops the strike-slip Kashi-Yecheng strike-slip fault and the compression-oriented main Pamir fault to the west, respectively. These three fault zones are used as boundaries to distinguish the Tarim Craton and the West Kunlun orogenic belt (Chen et al., 2018; Jiang et al., 2024). Paleoproterozoic, Neoproterozoic and Paleozoic rocks are widely exposed in the periphery of the fault zone, which is considered to be the main area for studying the Precambrian basement of the Tarim Basin (Zhang et al., 2004; Wang et al., 2015). At the same time, because of its special geographical location, the sedimentary rocks in the periphery of the fault zone have an indicative significance for the orogenic process of the West Kunlun orogenic belt. The core sampling point of this study is located in the Cretaceous strata of Kedong area in the northern part of Tiekelik Fault. The Cretaceous strata in Kedong area were continuously deposited on top of Jurassic, and there was no major angular unconformity in the middle. The Cretaceous mainly developed two subseries, the upper series is limited platform facies intertidal and tidal flat subfacies, the lower series is braided river delta facies, braided river delta front subfacies. According to the lithology, the upper Series is a set of carbonate rock and sand-mudstone deposits with local gravel. The lower series is a large set of sandstone and mudstone formations with gravel development in the middle and bottom. The Cretaceous strata are further divided into Upper Tuyiluoke Formation, Yigeziya Formation, Wuyitake Formation, Kukebai Formation and Lower Kezilesu Group from top to bottom (Figure 1C).

3 Sampling and methods

We took two samples from the kd5 well in the area, 5141.0 and 5409.4 respectively. Sample 5141.0 was collected from well kd5 at 5141.0 m. The formation is located in Kukebai Formation. The lithology of the sample is mainly fine sandstone. Sample 5409.4 was collected from well kd5 at 5409.4 m. The formation is located in the Kezilesu Formation. The lithologies of the sample are mainly fine sandstone and conglomerate.

More than 200 zircon particles were selected from the two sandstone samples after mechanical crushing, panning, magnetic separation and heavy fluid. Then, under the binocular, the zircon particles with complete crystal and clear and clean were fixed on the double-sided tape and arranged, and the target was injected with epoxy resin. Wait until the epoxy is fully cured and polish the zircon to the surface until the internal structure is fully revealed. The zircon target is then photographed by transparent/reflected light and cathodoluminescence (CL) to determine the internal structure of the zircon particles, avoiding cracks and inclusions in the zircon during the testing process. Zircon U-Pb dating was completed on the Laser denudation inductively coupled Plasma Mass Spectrometer (LA-ICP-MS) at the Laboratory of Basin Tectonics and Oil and Gas Accumulation, Petroleum Geology Experimental Research Center, Research Institute of Petroleum Exploration and Development, China. NWV 193 nm laser and Element SF-ICP-MS mass spectrometer are used. According to the image of cathode luminescence and reflection light, the denudation position was determined, the instrument signal was tuned by NIST614 to obtain the best test conditions, and the laser denudation parameters were determined, including the spot size of 30um and the denudation frequency of 3 Hz. In this study, 100 particles were randomly selected from two samples for analysis, making the number of analyzed particles consistent with statistical significance and able to reflect the source characteristics. For the selected denudation sites, every eight denudation sites are interlaced with a set of standard samples for data correction, including international standard zircon NIST610, 91,500 and PLE. Iolite software was used for baseline correction and blank deduction to form the final data. Finally, Isoplot4.15 software was used to calculate the age and make the graph. If the zircon age ≥1000 Ma is $^{207}Pb/^{206}Pb$, the zircon age ≤1000 Ma is $^{206}Pb/^{238}U$. When screening the valid data, the ratio of $^{206}Pb/^{238}U$ and $^{207}Pb/^{235}U$ is used as the selection criteria, and the compatibility degree greater than 90% is the valid data. Invalid data will not be considered in this study (The numbers in the table are marked in red). The complete analysis and test results, including zircon U-Pb isotope composition data and corresponding zircon age results, are shown in Tables 1, 2. (two points are deleted directly because they deviate too much from the harmonic line on the concordance diagram).

4 Results

4.1 Morphology and origin of detrital zircon

The morphological characteristics, internal structure characteristics and Th/U ratio of detrital zircon can reflect the characteristics and evolution of rock mass in provenance area (Li, 2009). The morphology of zircon is the most basic characteristic, which is manifested in the color of zircon, the length of zircon particles and the ratio of the length and axis of zircon particles (Hoskin and Schaltegger, 2003). In this study, a total of 200 detrital zircons from two samples were selected for U-Pb isotopic age testing, of which 157 zircons produced harmonic ages. The CL images of the two groups of samples generally show that the particle size of the zircons is between 50 and 300 μm, and the aspect ratio is about 1:1–1:3. Some zircons are angular-subangular-subcircular, and some zircons are subcircular (Figure 2). The former indicates that the transport distance is relatively close, which may be near-source deposition. The latter indicates that the Cretaceous zircons may have undergone multiple transport processes, which may be related to the long gap between the Cretaceous and zircon ages.

The internal structural features of zircon are primarily manifested in growth zoning. Growth zoning occurs as a result of episodic growth during zircon crystallization due to variations in fluid composition at different stages. Typical oscillating zoning is generally observed in magmatic zircons, whereas metamorphic zircons usually exhibit features such as unzoned or weakly zoned patterns and cloudy zoning (Wu and Zheng, 2004). In addition, the ratio of Th and U content in detrital zircons can also be used to judge the characteristics of zircons. Generally, the Th/U ratio of magmatic zircons is higher than 0.2, while the Th/U content ratio of metamorphic zircons is generally less than 0.1. Among the 157 detrital zircon samples, 151 zircons have Th/U > 0.2, accounting for 96.18 percent of the total (Figure 3). This indicates that basically all zircons have a high Th/U ratio (Th/U > 0.2), and the zircons in this experiment have obvious girding characteristics. Combined with the above morphological and structural analysis, it is shown that the samples we analyzed are basically from magmatic rocks, and the U-Pb age mainly indicates the crystallization time of zircon in magmatic activity. Therefore, the dating results provide constraints on the tectonic thermal time of different periods in the southwest Tarim and West Kunlun.

4.2 Detrital zircon geochronology

A total of 100 zircons were tested from well kd5 sample 5141.0, of which 22 zircons were determined as invalid ages (less than 90% concordant) due to serious loss of Pb content, and the remaining 78 zircons were determined as effective ages. The maximum age of zircon in this sample is 2548 Ma and the youngest is 255 Ma. The age distribution of U-Pb can be roughly divided into 510-255 Ma (N = 35, with an age peak of 460 Ma), 810–580 Ma (N = 16, no obvious peak), 1400-880 Ma (N = 15, no obvious peak), and 2,550–1,730 Ma (N = 12, no obvious peak). The majority of them were aged 510–255 Ma, accounting for 44.87%.

Sample 5490.4 from well kd5, a total of 100 zircons were tested, of which 21 zircons were determined to be effective ages (concordant degree greater than 90 percent) due to serious loss of Pb content. The maximum age of zircon in this sample is 2,524 Ma and the youngest is 208 Ma. The age distribution of U-Pb can be roughly divided into 380–208 Ma (N = 26, with an age peak of 260 Ma), 650–400 Ma (N = 46, with an age peak of 459 Ma), and 2,524-930 Ma (N = 7, without an obvious peak). The age group of 400–650 Ma accounts for 58.22%.

On the whole, the U-Pb ages of all concordant zircons can be roughly divided into five age groups: 290–208 Ma, 520–310 Ma, 810–580 Ma, 1,400–880 Ma and 2,548–1,730 Ma, of which the number of zircons in the 310-520 Ma age group accounts for 56.05%. There are two age peaks of 259 Ma and 459 Ma, which are similar to the respective age peaks of the two samples and can be used as the representative peaks of this sample (Figure 4).

TABLE 1 LA-ICP-MS U-Pb isotopic analysis data of zircon from Cretaceous 5141.0 sandstone in Kedong Area.

Spots	Isotopic ratios						Apparent age (Ma)								Concentratio			Concordant analyses
	$^{207}Pb/^{206}Pb$	2σ	$^{207}Pb/^{235}U$	2σ	$^{206}Pb/^{238}U$	2σ	$^{207}Pb/^{235}U$	2σ	$^{206}Pb/^{238}U$	2σ	$^{207}Pb/^{206}Pb$	2σ	Preferred age	2σ	U (ppm)	Th (ppm)	Th/U	
5141.0-1	0.06	0.01	0.62	0.12	0.08	0.01	474.69	82.15	476.22	49.84	206.79	480.53	476.22	49.84	164.62	90.23	0.55	1.00
5141.0-2	0.06	0.01	0.59	0.11	0.08	0.01	450.04	65.53	466.65	49.79	−4.62	425.71	466.65	49.79	356.97	197.62	0.55	0.96
5141.0-3	0.06	0.01	0.61	0.11	0.07	0.01	474.52	75.81	447.19	39.66	241.94	464.11	447.19	39.66	224.48	137.09	0.61	1.06
5141.0-4	0.11	0.01	5.80	0.86	0.38	0.04	1906.02	127.28	2035.31	181.25	1736.28	176.32	1736.28	176.32	168.93	363.16	2.15	0.94
5141.0-5	0.11	0.01	5.28	0.80	0.34	0.03	1823.13	124.76	1854.71	157.46	1751.90	166.33	1751.90	166.33	313.35	303.31	0.97	0.98
5141.0-6	0.07	0.01	1.81	0.34	0.18	0.02	982.96	123.19	1054.76	106.38	678.82	380.46	1054.76	106.38	75.49	79.10	1.05	0.93
5141.0-7	0.05	0.01	0.51	0.09	0.07	0.01	404.90	56.86	428.47	45.18	221.08	302.62	428.47	45.18	382.88	235.37	0.61	0.95
5141.0-8	0.05	0.01	0.57	0.08	0.08	0.01	451.10	55.32	466.10	40.30	252.34	256.26	466.10	40.30	537.60	289.82	0.54	0.97
5141.0-9	0.06	0.01	0.90	0.18	0.10	0.01	610.34	94.67	628.50	66.85	277.61	438.01	628.50	66.85	153.95	278.48	1.81	0.97
5141.0-10	0.16	0.01	10.17	1.52	0.47	0.05	2402.71	140.48	2414.72	214.11	2375.03	161.98	2375.03	161.98	121.14	75.44	0.62	1.00
5141.0-11	0.06	0.01	1.50	0.26	0.17	0.02	894.75	99.50	995.16	102.09	521.67	273.96	995.16	102.09	194.75	114.01	0.59	0.89
5141.0-12	0.06	0.01	0.57	0.11	0.07	0.01	448.44	72.06	459.04	44.70	285.24	349.28	459.04	44.70	247.08	171.26	0.69	0.98
5141.0-13	0.06	0.01	1.12	0.16	0.13	0.01	748.22	76.78	777.98	73.25	596.53	201.72	777.98	73.25	613.83	378.84	0.62	0.96
5141.0-14	0.08	0.01	1.78	0.33	0.18	0.02	996.19	124.63	1025.63	112.83	758.70	331.17	1025.63	112.83	141.59	216.45	1.53	0.97
5141.0-15	0.05	0.01	0.53	0.10	0.07	0.01	417.31	60.46	454.82	45.03	−94.56	481.03	454.82	45.03	342.79	279.93	0.82	0.92
5141.0-16	0.06	0.01	0.57	0.10	0.08	0.01	437.63	66.40	467.06	47.56	142.42	358.97	467.06	47.56	396.54	245.23	0.62	0.94
5141.0-17	0.06	0.01	0.57	0.09	0.08	0.01	455.16	61.41	468.31	50.42	264.61	264.25	468.31	50.42	566.42	264.60	0.47	0.97
5141.0-18	0.05	0.01	0.57	0.10	0.09	0.01	446.88	61.36	525.07	49.46	−29.20	322.55	525.07	49.46	485.60	195.11	0.40	0.85
5141.0-19	0.05	0.01	0.53	0.09	0.07	0.01	429.81	59.16	460.11	45.11	161.78	225.70	460.11	45.11	713.69	486.57	0.68	0.93

(Continued on the following page)

10.3389/feart.2024.1431866

TABLE 1 (*Continued*) LA-ICP-MS U-Pb isotopic analysis data of zircon from Cretaceous 5141.0 sandstone in Kedong Area.

Spots	Isotopic ratios						Apparent age (Ma)								Concentratio			Concordant analyses
	$^{207}Pb/^{206}Pb$	2σ	$^{207}Pb/^{235}U$	2σ	$^{206}Pb/^{238}U$	2σ	$^{207}Pb/^{235}U$	2σ	$^{206}Pb/^{238}U$	2σ	$^{207}Pb/^{206}Pb$	2σ	Preferred age	2σ	U (ppm)	Th (ppm)	Th/U	
5141.0-20	0.06	0.01	0.58	0.10	0.07	0.01	456.86	65.00	453.16	45.13	218.29	351.24	453.16	45.13	478.64	320.43	0.67	1.01
5141.0-21	0.07	0.01	1.63	0.26	0.18	0.02	951.34	99.28	1061.84	104.70	583.26	279.02	1061.84	104.70	224.20	201.15	0.90	0.89
5141.0-22	0.07	0.01	0.95	0.19	0.10	0.01	634.62	98.72	625.30	58.32	309.41	452.52	625.30	58.32	137.72	111.08	0.81	1.01
5141.0-23	0.16	0.01	10.80	1.54	0.50	0.05	2470.22	130.53	2548.23	208.82	2381.56	142.39	2548.23	208.82	518.07	255.68	0.49	0.97
5141.0-24	0.06	0.01	0.73	0.13	0.10	0.01	533.49	80.11	589.69	63.42	147.80	425.70	589.69	63.42	167.60	236.90	1.41	0.90
5141.0-25	0.05	0.01	0.48	0.10	0.07	0.01	377.63	67.41	456.94	48.51	30.39	359.38	456.94	48.51	230.97	142.43	0.62	0.83
5141.0-26	0.06	0.01	0.77	0.13	0.10	0.01	573.76	79.71	585.72	59.86	364.69	340.24	585.72	59.86	283.17	243.49	0.86	0.98
5141.0-27	0.06	0.01	0.68	0.14	0.08	0.01	491.90	82.87	479.31	48.72	542.85	440.08	479.31	48.72	140.35	118.82	0.85	1.03
5141.0-28	0.05	0.01	0.56	0.10	0.07	0.01	440.11	62.93	460.20	43.95	292.14	266.78	460.20	43.95	487.11	240.02	0.49	0.96
5141.0-29	0.06	0.01	0.57	0.09	0.07	0.01	447.83	59.93	461.91	40.42	238.05	315.92	461.91	40.42	339.04	194.40	0.57	0.97
5141.0-30	0.06	0.01	0.59	0.09	0.07	0.01	462.01	57.07	438.56	38.52	475.40	236.16	438.56	38.52	828.50	550.10	0.66	1.05
5141.0-31	0.05	0.01	0.52	0.08	0.08	0.01	422.15	60.88	484.63	47.02	54.26	345.36	484.63	47.02	309.99	208.51	0.67	0.87
5141.0-32	0.06	0.01	0.56	0.09	0.07	0.01	447.17	62.00	432.04	36.12	347.67	248.86	432.04	36.12	430.35	250.65	0.58	1.04
5141.0-33	0.06	0.01	0.57	0.11	0.07	0.01	438.00	69.69	423.14	36.82	450.56	314.00	423.14	36.82	262.63	150.92	0.57	1.04
5141.0-34	0.06	0.01	0.64	0.12	0.07	0.01	481.21	73.47	453.08	37.46	454.18	403.56	453.08	37.46	238.09	180.37	0.76	1.06
5141.0-35	0.06	0.01	0.55	0.08	0.07	0.01	436.42	52.29	450.81	37.83	303.32	290.74	450.81	37.83	517.09	261.62	0.51	0.97
5141.0-36	0.16	0.01	11.74	1.62	0.52	0.04	2553.25	133.06	2669.80	186.08	2420.78	148.10	2420.78	148.10	122.97	104.72	0.85	0.96
5141.0-37	0.06	0.01	0.65	0.11	0.08	0.01	487.83	68.92	500.82	47.61	268.81	373.05	500.82	47.61	201.24	90.13	0.45	0.97
5141.0-38	0.06	0.01	0.56	0.08	0.07	0.01	450.17	56.17	424.21	32.31	442.22	216.19	424.21	32.31	878.25	1237.53	1.41	1.06

(Continued on the following page)

10.3389/feart.2024.1431866

TABLE 1 (*Continued*) LA-ICP-MS U-Pb isotopic analysis data of zircon from Cretaceous 5141.0 sandstone in Kedong Area.

Spots	Isotopic ratios						Apparent age (Ma)								Concentratio			Concordant analyses
	$^{207}Pb/^{206}Pb$	2σ	$^{207}Pb/^{235}U$	2σ	$^{206}Pb/^{238}U$	2σ	$^{207}Pb/^{235}U$	2σ	$^{206}Pb/^{238}U$	2σ	$^{207}Pb/^{206}Pb$	2σ	Preferred age	2σ	U (ppm)	Th (ppm)	Th/U	
5141.0-39	0.06	0.01	0.57	0.10	0.07	0.01	441.36	62.94	446.17	36.96	306.11	350.62	446.17	36.96	240.20	141.10	0.59	0.99
5141.0-40	0.06	0.01	1.05	0.16	0.12	0.01	707.64	80.16	711.29	64.04	542.13	288.54	711.29	64.04	284.00	84.21	0.30	0.99
5141.0-41	0.07	0.01	0.66	0.11	0.07	0.01	499.24	67.05	448.40	35.20	478.45	305.14	448.40	35.20	548.57	312.75	0.57	1.11
5141.0-42	0.16	0.01	9.37	1.25	0.44	0.04	2363.79	134.63	2327.59	170.74	2388.07	135.67	2327.59	170.74	222.33	200.86	0.90	1.02
5141.0-43	0.07	0.01	0.95	0.21	0.10	0.01	620.49	105.62	625.02	63.59	311.94	469.53	625.02	63.59	129.48	59.81	0.46	0.99
5141.0-44	0.07	0.01	1.88	0.30	0.18	0.02	1041.30	102.84	1078.86	85.88	881.64	222.77	1078.86	85.88	190.97	71.31	0.37	0.97
5141.0-45	0.07	0.01	1.48	0.24	0.16	0.01	891.82	95.99	930.72	75.65	693.10	248.89	930.72	75.65	233.07	42.93	0.18	0.96
5141.0-46	0.14	0.01	6.61	0.98	0.35	0.03	2039.33	127.88	1896.12	161.69	2129.14	155.76	2129.14	155.76	161.22	158.56	0.98	1.08
5141.0-47	0.06	0.01	0.58	0.08	0.07	0.01	456.23	53.33	406.58	32.49	643.98	206.76	406.58	32.49	896.71	692.20	0.77	1.12
5141.0-48	0.05	0.01	0.51	0.09	0.07	0.01	404.62	55.38	459.30	40.44	−35.05	361.22	459.30	40.44	323.57	259.82	0.80	0.88
5141.0-49	0.06	0.01	0.55	0.09	0.07	0.01	452.22	71.75	447.66	38.48	267.09	351.48	447.66	38.48	271.93	181.79	0.67	1.01
5141.0-50	0.05	0.01	0.64	0.12	0.09	0.01	478.96	71.40	543.79	49.10	150.52	340.00	543.79	49.10	209.38	58.55	0.28	0.88
5141.0-51	0.07	0.02	1.01	0.30	0.11	0.01	624.14	159.78	688.05	63.53	1337.76	473.57	688.05	63.53	41.83	39.60	0.95	0.91
5141.0-52	0.06	0.01	0.93	0.15	0.11	0.01	649.24	79.00	669.41	60.54	429.37	316.82	669.41	60.54	268.57	34.94	0.13	0.97
5141.0-53	0.08	0.01	2.71	0.46	0.23	0.02	1275.05	123.70	1320.78	111.96	1130.66	249.79	1130.66	249.79	130.21	48.59	0.37	0.97
5141.0-54	0.06	0.01	0.33	0.06	0.04	0.00	281.05	44.52	255.71	26.25	278.23	378.67	255.71	26.25	643.15	243.85	0.38	1.09
5141.0-55	0.05	0.01	0.53	0.10	0.07	0.01	415.10	62.01	459.32	42.17	−46.50	419.38	459.32	42.17	254.44	163.23	0.64	0.90
5141.0-56	0.08	0.01	2.73	0.44	0.24	0.02	1288.88	124.08	1358.56	103.40	1043.76	242.02	1043.76	242.02	160.37	50.71	0.32	0.95
5141.0-57	0.06	0.01	1.32	0.20	0.15	0.01	836.21	86.77	889.86	66.01	624.69	205.76	889.86	66.01	464.14	38.07	0.08	0.94

(Continued on the following page)

10.3389/feart.2024.1431866

TABLE 1 (*Continued*) LA-ICP-MS U-Pb isotopic analysis data of zircon from Cretaceous 5141.0 sandstone in Kedong Area.

Spots	Isotopic ratios						Apparent age (Ma)								Concentratio			Concordant analyses
	$^{207}Pb/^{206}Pb$	2σ	$^{207}Pb/^{235}U$	2σ	$^{206}Pb/^{238}U$	2σ	$^{207}Pb/^{235}U$	2σ	$^{206}Pb/^{238}U$	2σ	$^{207}Pb/^{206}Pb$	2σ	Preferred age	2σ	U (ppm)	Th (ppm)	Th/U	
5141.0-58	0.07	0.01	1.48	0.22	0.16	0.01	903.45	87.18	947.38	76.81	720.70	198.11	947.38	76.81	400.95	233.57	0.58	0.95
5141.0-59	0.06	0.01	0.58	0.12	0.07	0.01	445.95	77.34	426.82	33.71	95.59	459.45	426.82	33.71	201.31	150.25	0.75	1.04
5141.0-60	0.07	0.01	1.02	0.18	0.12	0.01	683.80	87.50	697.42	61.87	468.93	296.76	697.42	61.87	217.67	213.69	0.98	0.98
5141.0-61	0.06	0.01	0.90	0.13	0.10	0.01	641.14	69.76	638.69	52.56	487.69	267.20	638.69	52.56	418.25	30.77	0.07	1.00
5141.0-62	0.08	0.01	2.29	0.40	0.22	0.02	1165.78	128.35	1255.27	114.35	737.52	434.97	1255.27	114.35	69.18	28.03	0.41	0.93
5141.0-63	0.12	0.01	5.04	0.70	0.30	0.03	1800.91	120.16	1686.22	130.37	1905.31	150.84	1905.31	150.84	247.41	181.34	0.73	1.07
5141.0-64	0.06	0.01	0.93	0.19	0.11	0.01	623.73	100.91	642.59	57.09	741.41	323.66	642.59	57.09	122.77	63.20	0.51	0.97
5141.0-65	0.05	0.01	0.54	0.11	0.07	0.01	419.39	68.67	457.92	40.15	−28.10	436.72	457.92	40.15	245.16	142.28	0.58	0.92
5141.0-66	0.06	0.01	0.89	0.13	0.11	0.01	639.54	74.28	645.90	49.67	567.98	236.39	645.90	49.67	525.43	60.37	0.11	0.99
5141.0-67	0.16	0.02	8.35	1.31	0.39	0.05	2244.13	138.73	2072.72	237.05	2379.97	202.19	2379.97	202.19	307.17	368.09	1.20	1.08
5141.0-68	0.06	0.01	0.59	0.09	0.08	0.01	461.71	58.40	470.10	39.16	199.98	329.10	470.10	39.16	438.53	244.06	0.56	0.98
5141.0-69	0.09	0.02	1.65	0.37	0.16	0.02	900.45	161.45	971.20	91.60	1018.51	434.59	971.20	91.60	43.86	53.32	1.22	0.93
5141.0-70	0.10	0.02	2.53	0.49	0.20	0.02	1223.91	160.66	1137.95	105.30	1395.48	320.66	1395.48	320.66	72.10	76.05	1.05	1.08
5141.0-71	0.06	0.01	0.61	0.10	0.07	0.01	481.73	64.81	450.90	37.26	520.61	293.01	450.90	37.26	357.06	210.61	0.59	1.07
5141.0-72	0.06	0.01	0.54	0.09	0.07	0.01	428.77	56.88	456.73	40.67	4.68	372.98	456.73	40.67	316.72	187.07	0.59	0.94
5141.0-73	0.07	0.01	1.61	0.24	0.17	0.01	951.69	94.93	989.28	77.30	763.52	222.52	989.28	77.30	272.49	492.30	1.81	0.96
5141.0-74	0.16	0.01	11.36	1.64	0.51	0.05	2514.10	134.81	2628.65	195.00	2389.18	165.82	2389.18	165.82	120.68	57.54	0.48	0.96

(Continued on the following page)

10.3389/feart.2024.1431866

TABLE 1 (*Continued*) LA-ICP-MS U-Pb isotopic analysis data of zircon from Cretaceous 5141.0 sandstone in Kedong Area.

Spots	Isotopic ratios						Apparent age (Ma)								Concentratio			Concordant analyses
	$^{207}Pb/^{206}Pb$	2σ	$^{207}Pb/^{235}U$	2σ	$^{206}Pb/^{238}U$	2σ	$^{207}Pb/^{235}U$	2σ	$^{206}Pb/^{238}U$	2σ	$^{207}Pb/^{206}Pb$	2σ	Preferred age	2σ	U (ppm)	Th (ppm)	Th/U	
5141.0-75	0.06	0.01	1.54	0.24	0.18	0.02	920.41	94.17	1058.15	92.12	487.01	258.26	1058.15	92.12	263.35	6.56	0.02	0.87
5141.0-77	0.07	0.01	1.77	0.27	0.19	0.02	1018.53	101.64	1105.30	99.01	787.98	265.01	1105.30	99.01	246.98	74.30	0.30	0.92
5141.0-78	0.05	0.01	0.33	0.06	0.05	0.01	280.37	46.24	337.34	32.07	−486.67	456.29	337.34	32.07	359.61	147.99	0.41	0.83
5141.0-79	0.05	0.01	0.55	0.09	0.08	0.01	432.50	57.10	490.19	47.36	−80.73	330.55	490.19	47.36	506.60	308.05	0.61	0.88
5141.0-80	0.07	0.01	1.58	0.25	0.17	0.02	932.49	96.69	983.39	94.31	703.88	286.99	983.39	94.31	227.38	169.19	0.74	0.95
5141.0-81	0.12	0.01	5.98	0.86	0.37	0.04	1939.53	127.05	1977.67	177.81	1891.80	174.27	1891.80	174.27	167.91	53.87	0.32	0.98
5141.0-82	0.06	0.01	0.59	0.11	0.08	0.01	448.16	69.73	469.47	44.28	233.91	392.26	469.47	44.28	211.82	151.04	0.71	0.95
5141.0-83	0.06	0.01	0.82	0.18	0.11	0.01	560.51	100.80	640.68	72.67	335.51	491.46	640.68	72.67	108.97	199.38	1.83	0.87
5141.0-84	0.07	0.01	1.23	0.25	0.13	0.01	768.95	116.33	809.20	86.96	362.89	512.15	809.20	86.96	78.30	40.51	0.52	0.95
5141.0-85	0.05	0.01	0.53	0.08	0.08	0.01	424.56	53.32	468.52	44.53	4.37	344.02	468.52	44.53	579.55	294.72	0.51	0.91
5141.0-86	0.06	0.01	1.05	0.21	0.13	0.02	689.16	114.86	783.66	84.95	387.11	379.98	783.66	84.95	92.61	59.37	0.64	0.88
5141.0-87	0.06	0.01	0.62	0.11	0.08	0.01	467.83	73.95	465.84	45.67	464.31	350.42	465.84	45.67	244.37	152.80	0.63	1.00
5141.0-88	0.05	0.01	0.52	0.10	0.08	0.01	411.26	63.09	472.32	47.58	−110.52	413.14	472.32	47.58	385.15	253.36	0.66	0.87
5141.0-89	0.05	0.01	0.49	0.09	0.07	0.01	390.91	59.34	458.93	43.63	−0.78	324.91	458.93	43.63	337.80	223.03	0.66	0.85
5141.0-90	0.12	0.01	6.34	0.92	0.37	0.03	1986.07	133.00	2005.66	161.62	1941.96	157.42	2005.66	161.62	130.93	49.26	0.38	0.99
5141.0-91	0.06	0.01	0.85	0.14	0.10	0.01	618.35	80.18	616.43	53.95	504.39	244.85	616.43	53.95	361.40	311.77	0.86	1.00

(Continued on the following page)

10.3389/feart.2024.1431866

TABLE 1 (*Continued*) LA-ICP-MS U-Pb isotopic analysis data of zircon from Cretaceous 5141.0 sandstone in Kedong Area.

Spots	Isotopic ratios						Apparent age (Ma)								Concentratio			Concordant analyses
	$^{207}Pb/^{206}Pb$	2σ	$^{207}Pb/^{235}U$	2σ	$^{206}Pb/^{238}U$	2σ	$^{207}Pb/^{235}U$	2σ	$^{206}Pb/^{238}U$	2σ	$^{207}Pb/^{206}Pb$	2σ	Preferred age	2σ	U (ppm)	Th (ppm)	Th/U	
5141.0-92	0.06	0.01	0.63	0.10	0.08	0.01	485.51	60.04	505.53	46.71	224.27	322.37	505.53	46.71	820.32	380.95	0.46	0.96
5141.0-94	0.09	0.01	3.88	0.58	0.31	0.03	1573.98	120.82	1698.77	136.28	1396.58	170.72	1396.58	170.72	222.52	73.46	0.33	0.93
5141.0-95	0.09	0.02	1.24	0.28	0.11	0.01	754.59	128.68	650.58	77.22	1174.68	408.28	650.58	77.22	111.75	134.50	1.20	1.16
5141.0-96	0.06	0.01	0.83	0.14	0.10	0.01	601.68	83.60	611.07	53.87	343.96	338.79	611.07	53.87	259.61	359.24	1.38	0.98
5141.0-97	0.06	0.01	1.39	0.22	0.17	0.02	869.48	98.43	986.94	90.45	472.24	242.61	986.94	90.45	336.76	193.90	0.58	0.88
5141.0-98	0.06	0.01	0.58	0.09	0.07	0.01	450.28	60.26	460.41	41.73	239.91	304.87	460.41	41.73	473.21	300.62	0.64	0.98
5141.0-99	0.05	0.01	0.52	0.10	0.08	0.01	408.11	63.72	472.80	48.68	106.00	313.42	472.80	48.68	368.51	245.27	0.67	0.86
5141.0-100	0.05	0.01	0.47	0.07	0.07	0.01	382.14	49.60	431.22	43.74	106.98	268.35	431.22	43.74	779.67	249.62	0.32	0.89

10.3389/feart.2024.1431866

TABLE 2 LA-ICP-MS U-Pb isotopic analysis data of zircon from Cretaceous 5409.4 sandstone in Kedong Area.

Spots	Isotopic ratios						Apparent age (Ma)								Concentratio			Concordant analyses
	$^{207}Pb/^{206}Pb$	2σ	$^{207}Pb/^{235}U$	2σ	$^{206}Pb/^{238}U$	2σ	$^{207}Pb/^{235}U$	2σ	$^{206}Pb/^{238}U$	2σ	$^{207}Pb/^{206}Pb$	2σ	Preferred age	2σ	U (ppm)	Th (ppm)	Th/U	
5409.4-1	0.07	0.01	1.69	0.29	0.18	0.02	969.58	123.02	1033.53	106.58	884.44	298.51	1033.53	106.58	124.96	53.85	0.43	0.94
5409.4-2	0.06	0.01	0.59	0.11	0.07	0.01	451.46	67.96	461.93	50.35	212.23	346.95	461.93	50.35	305.04	162.18	0.53	0.98
5409.4-3	0.05	0.01	0.26	0.05	0.03	0.00	228.80	38.74	208.33	19.56	204.28	365.36	208.33	19.56	638.54	273.77	0.43	1.09
5409.4-4	0.05	0.01	0.37	0.07	0.05	0.01	308.18	49.35	313.72	33.17	92.46	356.45	313.72	33.17	474.90	323.77	0.68	0.98
5409.4-5	0.06	0.01	0.32	0.08	0.05	0.01	272.00	61.56	283.69	36.21	512.24	422.10	283.69	36.21	174.91	169.55	0.97	0.96
5409.4-6	0.05	0.01	0.58	0.10	0.08	0.01	451.35	63.16	491.24	48.50	105.01	335.87	491.24	48.50	395.86	190.64	0.48	0.92
5409.4-7	0.05	0.01	0.56	0.12	0.08	0.01	420.53	78.53	475.22	47.86	4.27	450.51	475.22	47.86	145.77	112.56	0.77	0.88
5409.4-8	0.05	0.01	0.51	0.09	0.08	0.01	410.37	57.15	480.43	54.13	−186.89	373.19	480.43	54.13	523.68	284.92	0.54	0.85
5409.4-9	0.07	0.02	0.53	0.19	0.06	0.01	368.85	117.52	348.00	48.55	2035.40	379.66	348.00	48.55	46.08	27.34	0.59	1.06
5409.4-10	0.06	0.01	0.61	0.11	0.08	0.01	467.19	70.31	470.02	51.55	464.73	362.84	470.02	51.55	155.47	92.28	0.59	0.99
5409.4-11	0.06	0.01	0.66	0.11	0.08	0.01	501.46	63.85	479.87	47.24	536.81	264.76	479.87	47.24	383.52	257.10	0.67	1.04
5409.4-12	0.05	0.01	0.55	0.12	0.07	0.01	415.10	74.97	464.06	42.78	85.16	405.27	464.06	42.78	157.38	50.41	0.32	0.89
5409.4-13	0.05	0.01	0.33	0.05	0.05	0.00	279.98	41.40	289.63	27.94	−68.72	389.69	289.63	27.94	650.78	348.20	0.54	0.97
5409.4-14	0.06	0.01	0.58	0.10	0.08	0.01	451.76	63.22	474.01	50.57	395.36	279.18	474.01	50.57	438.21	242.61	0.55	0.95
5409.4-15	0.06	0.01	0.56	0.11	0.08	0.01	428.80	67.11	467.25	47.43	86.80	398.43	467.25	47.43	265.27	131.28	0.49	0.92
5409.4-16	0.06	0.01	0.37	0.09	0.05	0.01	296.45	65.81	311.31	35.63	305.25	516.57	311.31	35.63	177.60	76.95	0.43	0.95
5409.4-17	0.05	0.01	0.52	0.09	0.08	0.01	424.66	59.82	476.68	47.38	7.64	294.76	476.68	47.38	659.38	389.57	0.59	0.89
5409.4-18	0.05	0.01	0.29	0.05	0.04	0.00	260.66	45.34	264.52	25.80	−44.23	455.35	264.52	25.80	348.37	209.38	0.60	0.99
5409.4-19	0.06	0.01	0.41	0.09	0.06	0.01	341.19	65.96	365.26	36.01	−84.92	510.06	365.26	36.01	212.12	72.32	0.34	0.93

(Continued on the following page)

10.3389/feart.2024.1431866

TABLE 2 (*Continued*) LA-ICP-MS U-Pb isotopic analysis data of zircon from Cretaceous 5409.4 sandstone in Kedong Area.

Spots	Isotopic ratios						Apparent age (Ma)								Concentratio			Concordant analyses
	$^{207}Pb/^{206}Pb$	2σ	$^{207}Pb/^{235}U$	2σ	$^{206}Pb/^{238}U$	2σ	$^{207}Pb/^{235}U$	2σ	$^{206}Pb/^{238}U$	2σ	$^{207}Pb/^{206}Pb$	2σ	Preferred age	2σ	U (ppm)	Th (ppm)	Th/U	
5409.4-20	0.05	0.01	0.56	0.13	0.07	0.01	413.60	79.82	461.15	48.45	145.18	486.52	461.15	48.45	221.92	99.79	0.45	0.89
5409.4-21	0.05	0.01	0.52	0.10	0.08	0.01	413.09	59.46	466.02	46.41	128.61	303.08	466.02	46.41	374.92	226.58	0.60	0.89
5409.4-22	0.07	0.01	0.45	0.10	0.05	0.01	359.04	77.86	326.25	32.62	860.22	450.85	326.25	32.62	171.88	141.42	0.82	1.11
5409.4-23	0.06	0.01	0.61	0.12	0.08	0.01	470.32	77.97	486.35	52.92	183.58	425.44	486.35	52.92	247.11	138.95	0.56	0.97
5409.4-24	0.06	0.01	0.57	0.11	0.08	0.01	446.17	73.94	466.32	45.91	231.63	348.58	466.32	45.91	223.10	125.57	0.56	0.96
5409.4-25	0.06	0.01	0.33	0.07	0.04	0.00	278.45	50.87	238.73	24.12	452.59	428.39	238.73	24.12	346.24	273.38	0.79	1.17
5409.4-26	0.05	0.01	0.45	0.07	0.07	0.01	373.11	53.85	409.26	39.30	−28.73	392.19	409.26	39.30	517.55	452.15	0.87	0.91
5409.4-27	0.06	0.01	0.49	0.10	0.06	0.01	377.82	69.58	357.34	33.07	349.54	404.96	357.34	33.07	177.69	111.31	0.63	1.06
5409.4-28	0.06	0.01	0.52	0.09	0.07	0.01	416.63	64.92	427.69	41.70	143.70	393.59	427.69	41.70	328.79	240.09	0.73	0.97
5409.4-29	0.06	0.02	0.39	0.10	0.06	0.01	318.11	77.80	350.97	39.96	928.65	389.97	350.97	39.96	113.12	33.84	0.30	0.91
5409.4-30	0.06	0.01	0.50	0.15	0.06	0.01	358.01	93.49	373.80	44.21	1161.60	331.95	373.80	44.21	74.06	31.24	0.42	0.96
5409.4-31	0.05	0.01	0.25	0.04	0.04	0.00	221.72	35.28	256.71	23.07	−382.78	367.26	256.71	23.07	618.04	314.84	0.51	0.86
5409.4-32	0.06	0.01	0.57	0.09	0.07	0.01	442.15	62.70	421.28	37.59	567.24	255.95	421.28	37.59	287.44	101.51	0.35	1.05
5409.4-33	0.17	0.01	12.78	1.79	0.54	0.04	2632.15	127.12	2728.46	176.06	2524.71	150.31	2524.71	150.31	118.48	80.13	0.68	0.96
5409.4-34	0.06	0.01	0.57	0.08	0.07	0.01	460.78	56.73	456.96	36.32	367.10	232.13	456.96	36.32	683.91	458.76	0.67	1.01
5409.4-35	0.06	0.01	0.35	0.08	0.04	0.00	283.46	60.55	277.67	26.48	494.25	460.92	277.67	26.48	201.82	103.23	0.51	1.02
5409.4-36	0.09	0.01	2.78	0.40	0.23	0.02	1322.11	111.39	1318.98	105.16	1317.35	185.12	1317.35	185.12	249.91	78.46	0.31	1.00
5409.4-37	0.06	0.02	0.58	0.17	0.07	0.01	415.16	110.50	448.89	51.28	1305.55	448.63	448.89	51.28	73.30	92.01	1.26	0.92

(Continued on the following page)

10.3389/feart.2024.1431866

TABLE 2 (*Continued*) LA-ICP-MS U-Pb isotopic analysis data of zircon from Cretaceous 5409.4 sandstone in Kedong Area.

Spots	Isotopic ratios						Apparent age (Ma)								Concentratio			Concordant analyses
	$^{207}Pb/^{206}Pb$	2σ	$^{207}Pb/^{235}U$	2σ	$^{206}Pb/^{238}U$	2σ	$^{207}Pb/^{235}U$	2σ	$^{206}Pb/^{238}U$	2σ	$^{207}Pb/^{206}Pb$	2σ	Preferred age	2σ	U (ppm)	Th (ppm)	Th/U	
5409.4-38	0.06	0.01	0.62	0.12	0.07	0.01	470.49	84.62	440.45	40.49	388.49	404.12	440.45	40.49	136.28	76.29	0.56	1.07
5409.4-39	0.05	0.01	0.57	0.09	0.07	0.01	445.21	57.53	461.86	34.93	216.78	254.92	461.86	34.93	623.51	367.26	0.59	0.96
5409.4-40	0.06	0.01	0.63	0.11	0.08	0.01	479.64	68.03	469.25	42.03	295.37	411.19	469.25	42.03	261.46	115.87	0.44	1.02
5409.4-41	0.06	0.01	0.31	0.06	0.04	0.00	275.07	46.95	256.89	27.08	110.37	493.99	256.89	27.08	357.14	181.93	0.51	1.07
5409.4-42	0.05	0.01	0.64	0.11	0.08	0.01	485.16	69.56	512.82	43.28	53.81	379.75	512.82	43.28	267.28	159.56	0.60	0.95
5409.4-43	0.06	0.01	0.52	0.08	0.07	0.01	422.79	57.29	428.37	34.56	198.33	275.42	428.37	34.56	650.53	383.85	0.59	0.99
5409.4-44	0.06	0.02	0.30	0.09	0.04	0.00	241.84	65.12	236.18	23.48	1034.75	444.73	236.18	23.48	163.75	114.54	0.70	1.02
5409.4-45	0.06	0.01	0.62	0.11	0.08	0.01	470.23	68.16	471.79	44.70	346.03	412.48	471.79	44.70	243.23	164.17	0.67	1.00
5409.4-46	0.07	0.01	1.76	0.29	0.18	0.02	989.31	113.09	1053.85	88.66	839.26	258.49	1053.85	88.66	186.88	154.88	0.83	0.94
5409.4-47	0.05	0.01	0.57	0.10	0.08	0.01	437.63	66.23	508.91	43.19	153.66	301.59	508.91	43.19	294.96	137.98	0.47	0.86
5409.4-48	0.05	0.01	0.52	0.09	0.07	0.01	416.33	58.63	428.93	38.90	327.78	267.07	428.93	38.90	294.95	147.14	0.50	0.97
5409.4-49	0.07	0.02	0.39	0.10	0.04	0.00	299.52	73.40	254.55	22.91	1077.29	453.09	254.55	22.91	161.42	103.42	0.64	1.18
5409.4-50	0.06	0.01	0.64	0.11	0.07	0.01	486.57	67.33	462.01	38.46	372.58	382.51	462.01	38.46	256.90	204.21	0.79	1.05
5409.4-51	0.05	0.01	0.53	0.08	0.07	0.01	420.60	55.31	459.79	36.78	208.64	253.32	459.79	36.78	670.54	369.30	0.55	0.91
5409.4-52	0.07	0.01	1.35	0.27	0.16	0.02	827.48	125.23	945.61	101.15	640.41	344.90	945.61	101.15	54.30	23.13	0.43	0.88
5409.4-53	0.06	0.01	0.56	0.09	0.08	0.01	444.05	64.52	466.50	46.69	144.59	424.95	466.50	46.69	242.66	144.65	0.60	0.95
5409.4-54	0.05	0.01	0.30	0.06	0.04	0.00	255.01	44.27	265.21	26.14	138.61	326.25	265.21	26.14	447.84	274.57	0.61	0.96
5409.4-55	0.05	0.01	0.49	0.09	0.07	0.01	390.36	59.17	426.90	37.83	−212.36	442.61	426.90	37.83	340.82	138.84	0.41	0.91

(Continued on the following page)

10.3389/feart.2024.1431866

TABLE 2 (*Continued*) LA-ICP-MS U-Pb isotopic analysis data of zircon from Cretaceous 5409.4 sandstone in Kedong Area.

Spots	Isotopic ratios						Apparent age (Ma)								Concentratio			Concordant analyses
	$^{207}Pb/^{206}Pb$	2σ	$^{207}Pb/^{235}U$	2σ	$^{206}Pb/^{238}U$	2σ	$^{207}Pb/^{235}U$	2σ	$^{206}Pb/^{238}U$	2σ	$^{207}Pb/^{206}Pb$	2σ	Preferred age	2σ	U (ppm)	Th (ppm)	Th/U	
5409.4-56	0.07	0.02	0.38	0.09	0.04	0.00	310.91	68.01	275.10	29.31	592.91	517.44	275.10	29.31	195.64	142.23	0.73	1.13
5409.4-57	0.05	0.01	0.47	0.09	0.07	0.01	383.74	63.99	415.40	37.73	32.74	370.06	415.40	37.73	324.02	61.75	0.19	0.92
5409.4-58	0.05	0.01	0.52	0.09	0.07	0.01	422.37	65.29	433.38	36.35	173.30	328.95	433.38	36.35	326.71	208.37	0.64	0.97
5409.4-59	0.12	0.01	4.64	0.64	0.29	0.03	1732.62	117.95	1645.77	133.24	1824.01	173.23	1824.01	173.23	247.36	90.36	0.37	1.05
5409.4-60	0.05	0.01	0.24	0.05	0.04	0.00	227.08	50.98	226.16	22.64	120.51	445.67	226.16	22.64	297.52	297.24	1.00	1.00
5409.4-61	0.05	0.01	0.53	0.08	0.07	0.01	421.82	56.94	437.93	39.68	322.60	226.45	437.93	39.68	583.76	338.40	0.58	0.96
5409.4-62	0.06	0.01	0.30	0.06	0.04	0.00	261.92	49.32	252.73	21.19	268.71	418.31	252.73	21.19	376.96	335.69	0.89	1.04
5409.4-63	0.06	0.01	0.92	0.19	0.11	0.01	620.09	97.52	643.87	59.15	373.77	467.54	643.87	59.15	117.13	88.20	0.75	0.96
5409.4-64	0.16	0.01	10.58	1.53	0.49	0.05	2446.33	136.11	2535.91	196.13	2362.55	135.80	2362.55	135.80	171.65	59.43	0.35	0.96
5409.4-65	0.06	0.01	0.61	0.09	0.08	0.01	473.70	57.68	489.11	46.16	375.27	267.13	489.11	46.16	426.68	160.49	0.38	0.97
5409.4-66	0.06	0.01	0.32	0.07	0.04	0.00	276.08	56.28	264.67	23.25	407.65	433.82	264.67	23.25	235.47	109.91	0.47	1.04
5409.4-67	0.06	0.01	0.57	0.10	0.08	0.01	450.81	68.50	478.92	45.24	162.82	387.68	478.92	45.24	269.57	161.43	0.60	0.94
5409.4-68	0.05	0.01	0.26	0.04	0.04	0.00	233.35	34.90	247.45	23.98	63.50	313.87	247.45	23.98	938.93	417.01	0.44	0.94
5409.4-69	0.06	0.01	0.53	0.10	0.07	0.01	414.56	61.71	417.63	41.47	334.52	357.43	417.63	41.47	248.54	87.12	0.35	0.99
5409.4-70	0.06	0.01	0.29	0.05	0.04	0.00	262.29	49.61	260.98	27.33	247.86	363.83	260.98	27.33	435.15	241.83	0.56	1.01
5409.4-71	0.05	0.01	0.51	0.08	0.08	0.01	410.34	54.89	469.23	40.78	−141.18	395.68	469.23	40.78	514.41	300.28	0.58	0.87
5409.4-72	0.06	0.01	0.60	0.14	0.07	0.01	439.10	84.97	441.79	47.99	366.97	534.21	441.79	47.99	173.53	99.96	0.58	0.99
5409.4-73	0.06	0.01	0.68	0.12	0.08	0.01	507.28	73.31	490.00	46.85	389.77	375.60	490.00	46.85	190.03	120.70	0.64	1.04
5409.4-74	0.06	0.01	0.67	0.16	0.08	0.01	467.99	94.86	465.26	43.26	510.83	478.69	465.26	43.26	119.66	77.75	0.65	1.01

(Continued on the following page)

10.3389/feart.2024.1431866

TABLE 2 (*Continued*) LA-ICP-MS U-Pb isotopic analysis data of zircon from Cretaceous 5409.4 sandstone in Kedong Area.

Spots	Isotopic ratios						Apparent age (Ma)								Concentratio			Concordant analyses
	$^{207}Pb/^{206}Pb$	2σ	$^{207}Pb/^{235}U$	2σ	$^{206}Pb/^{238}U$	2σ	$^{207}Pb/^{235}U$	2σ	$^{206}Pb/^{238}U$	2σ	$^{207}Pb/^{206}Pb$	2σ	Preferred age	2σ	U (ppm)	Th (ppm)	Th/U	
5409.4-75	0.08	0.02	0.38	0.09	0.04	0.00	305.54	66.40	259.74	29.51	1033.27	452.41	259.74	29.51	177.47	88.74	0.50	1.18
5409.4-76	0.05	0.01	0.59	0.12	0.08	0.01	453.54	83.04	488.56	47.40	28.98	425.99	488.56	47.40	194.41	76.33	0.39	0.93
5409.4-77	0.06	0.01	0.38	0.07	0.05	0.01	320.46	46.58	320.56	34.57	211.61	334.22	320.56	34.57	483.50	227.90	0.47	1.00
5409.4-78	0.05	0.01	0.53	0.11	0.07	0.01	408.98	70.84	442.60	45.18	−37.70	508.23	442.60	45.18	227.76	95.21	0.42	0.92
5409.4-79	0.07	0.01	0.45	0.09	0.05	0.01	368.42	65.99	327.53	37.34	681.52	358.42	327.53	37.34	240.32	53.52	0.22	1.12
5409.4-80	0.06	0.01	0.32	0.08	0.04	0.00	270.76	59.85	251.34	26.99	185.54	486.76	251.34	26.99	266.66	168.92	0.63	1.08
5409.4-81	0.05	0.02	0.36	0.12	0.05	0.01	272.79	80.68	313.54	35.47	1408.48	420.95	313.54	35.47	79.46	47.99	0.60	0.87
5409.4-82	0.06	0.01	0.39	0.08	0.05	0.01	327.14	65.74	327.96	37.57	436.37	434.29	327.96	37.57	179.28	70.76	0.39	1.00
5409.4-83	0.05	0.01	0.31	0.06	0.04	0.00	264.20	45.68	281.80	30.42	−37.63	393.43	281.80	30.42	412.76	235.64	0.57	0.94
5409.4-84	0.06	0.01	0.56	0.09	0.07	0.01	447.04	65.53	462.33	49.50	245.72	408.81	462.33	49.50	338.35	119.10	0.35	0.97
5409.4-85	0.07	0.02	0.35	0.11	0.04	0.00	267.30	77.02	245.41	26.68	1537.00	425.71	245.41	26.68	112.86	130.01	1.15	1.09
5409.4-86	0.05	0.01	0.49	0.08	0.07	0.01	412.13	62.75	421.16	42.67	296.75	260.68	421.16	42.67	444.05	240.22	0.54	0.98
5409.4-87	0.06	0.02	0.55	0.17	0.08	0.01	389.91	111.12	486.45	54.84	1162.78	506.65	486.45	54.84	57.64	28.82	0.50	0.80
5409.4-88	0.06	0.01	0.56	0.10	0.07	0.01	434.17	65.06	449.78	38.90	272.25	334.26	449.78	38.90	325.99	209.06	0.64	0.97
5409.4-89	0.05	0.01	0.28	0.06	0.04	0.00	245.24	50.61	280.92	29.54	−229.59	478.69	280.92	29.54	242.75	118.32	0.49	0.87
5409.4-90	0.06	0.01	0.57	0.10	0.07	0.01	440.36	65.37	449.61	44.07	400.55	362.38	449.61	44.07	319.51	216.39	0.68	0.98
5409.4-91	0.06	0.01	0.29	0.06	0.04	0.00	252.94	44.51	246.39	24.77	208.45	378.10	246.39	24.77	590.45	173.89	0.29	1.03

(Continued on the following page)

10.3389/feart.2024.1431866

TABLE 2 (*Continued*) LA-ICP-MS U-Pb isotopic analysis data of zircon from Cretaceous 5409.4 sandstone in Kedong Area.

Spots	Isotopic ratios						Apparent age (Ma)								Concentratio			Concordant analyses
	$^{207}Pb/^{206}Pb$	2σ	$^{207}Pb/^{235}U$	2σ	$^{206}Pb/^{238}U$	2σ	$^{207}Pb/^{235}U$	2σ	$^{206}Pb/^{238}U$	2σ	$^{207}Pb/^{206}Pb$	2σ	Preferred age	2σ	U (ppm)	Th (ppm)	Th/U	
5409.4-92	0.06	0.01	0.57	0.10	0.07	0.01	452.46	67.96	447.78	43.99	339.52	379.18	447.78	43.99	233.22	133.77	0.57	1.01
5409.4-93	0.06	0.01	0.55	0.10	0.08	0.01	430.40	62.85	465.62	47.08	−35.37	417.80	465.62	47.08	282.85	163.78	0.58	0.92
5409.4-94	0.05	0.01	0.24	0.04	0.04	0.00	210.25	33.14	238.71	23.97	−398.68	397.40	238.71	23.97	810.67	621.92	0.77	0.88
5409.4-95	0.05	0.01	0.33	0.08	0.05	0.01	271.84	57.60	330.47	30.73	−430.43	538.31	330.47	30.73	191.77	124.98	0.65	0.82
5409.4-96	0.06	0.01	0.63	0.12	0.07	0.01	469.83	73.51	452.88	45.69	477.07	365.00	452.88	45.69	203.92	68.97	0.34	1.04
5409.4-97	0.05	0.01	0.48	0.09	0.07	0.01	394.55	63.78	431.00	40.09	80.78	364.08	431.00	40.09	286.88	170.57	0.59	0.92
5409.4-98	0.06	0.01	1.45	0.24	0.16	0.01	875.17	98.00	935.17	83.20	681.28	229.24	935.17	83.20	319.02	151.71	0.48	0.94
5409.4-99	0.06	0.01	0.58	0.10	0.07	0.01	458.37	69.73	463.32	43.01	375.00	346.31	463.32	43.01	365.35	130.56	0.36	0.99
5409.4-100	0.05	0.01	0.52	0.08	0.07	0.01	420.80	50.49	439.00	40.30	292.61	227.57	439.00	40.30	879.85	509.50	0.58	0.96

10.3389/feart.2024.1431866

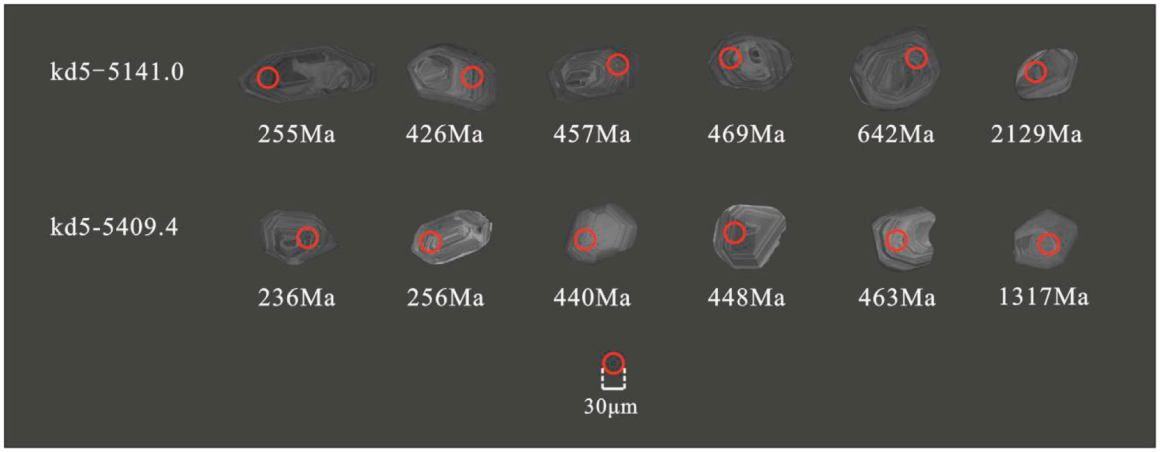

FIGURE 2
Representative CL images of zircon grains in this study. The U-Pb analysis spots (30 μm) are displayed by solid circles.

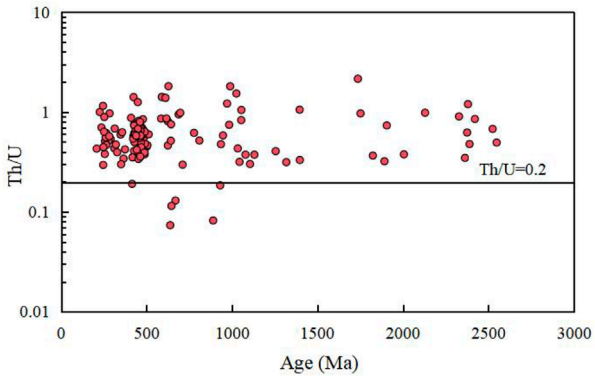

FIGURE 3
Th/U and ages for zircons analyzed in this study.

5 Discussion

5.1 Detrital zircon geochronology

The zircons obtained in this study range in age from Paleoproterozoic to Triassic. The study area is located at the junction of the Tarim Basin and the West Kunlun orogenic belt, indicating that the detrital zircons in this study mainly come from the sedimentary strata in the Tarim Basin and the Tethys tectonic domain. At the same time, due to the limited activities of the Precambrian Tethys, the age of the pre-Paleozoic zircons should be strongly consistent with the tectonic thermal events in the Tarim Basin. At the same time, the Precambrian tectonic movement of the peripheral terranes of the piedmont belt cannot be ruled out because the terranes inside the West Kunlun orogenic belt all have Precambrian strata.

The results show that a global continental accretion event occurred around 2,500 Ma, and magmatic records of this stage have been found in North China, South China, West Africa and Northern Finland. Zircons from this period are widely distributed in the Tarim Basin and its periphery, mainly in the Kuruktag and Tiekelik areas. Zircons of this age in this study should be the records of this accretion event (Shu et al., 2011; Ge et al., 2022). Whether the Tarim Basin participated in the converging of the Columbia supercontinent in the Paleoproterozoic period after 2,000 Ma is a mystery, because the magmatic activity of this tectonic event is rarely recorded in and around the Tarim Basin, such as the 1.87 Ga quartz syenite with A-type granite characteristics found in the Altyn area in the southeast margin of the Tarim Basin (Xin et al., 2011). In this study, the number of zircons in this age group is still small, which is presumed to come from a small number of volcanic records in the Tarim Basin and its surroundings. During the Mesoproterozoic era, the Tarim Craton widely received passive continental margin sediments, with a small number of zircon ages distributed between 1,500–1,000 Ma. These zircons mainly originated from intraplate volcanic tectonic activity. During the Neoproterozoic period, the Tarim Basin participated in the aggregation of the Rodinia supercontinent, because related magmatic and metamorphic rocks were widely distributed in the Tarim Basin and its surrounding areas. For example, Zhang et al. (2003); Zhang et al. (2007) determined the age of 1.2 Ga of the Liancate Group igneous rocks in Southwest Tarim by using the Sm-Nd isochron method. At the same time, the age of 1.05 Ga of metamorphic hornblende in this area was also determined by $^{40}Ar/^{39}Ar$ (Zhang et al., 2003; Zhang et al., 2007), zircons at 1300 Ma to 900 Ma should come from here. The detrital zircon sample contains more zircons from 600 to 900 Ma, which corresponds to the previous thought that the Tarim Basin participated in the cracking process of the Rodinia supercontinent, and a large number of magmatic activities at this age have been recorded in the Tarim Basin. For example, Kuluktag, Aksu, and Tiekelik have extensively developed bimodal volcanism, mafic dike swarms, and alkaline granites, all around 800 Ma which are the sources of zircons in this age group in this experiment (Zhu et al., 2008; Xu et al., 2009; Long et al., 2011; Zhang et al., 2011; Zhang et al., 2013).

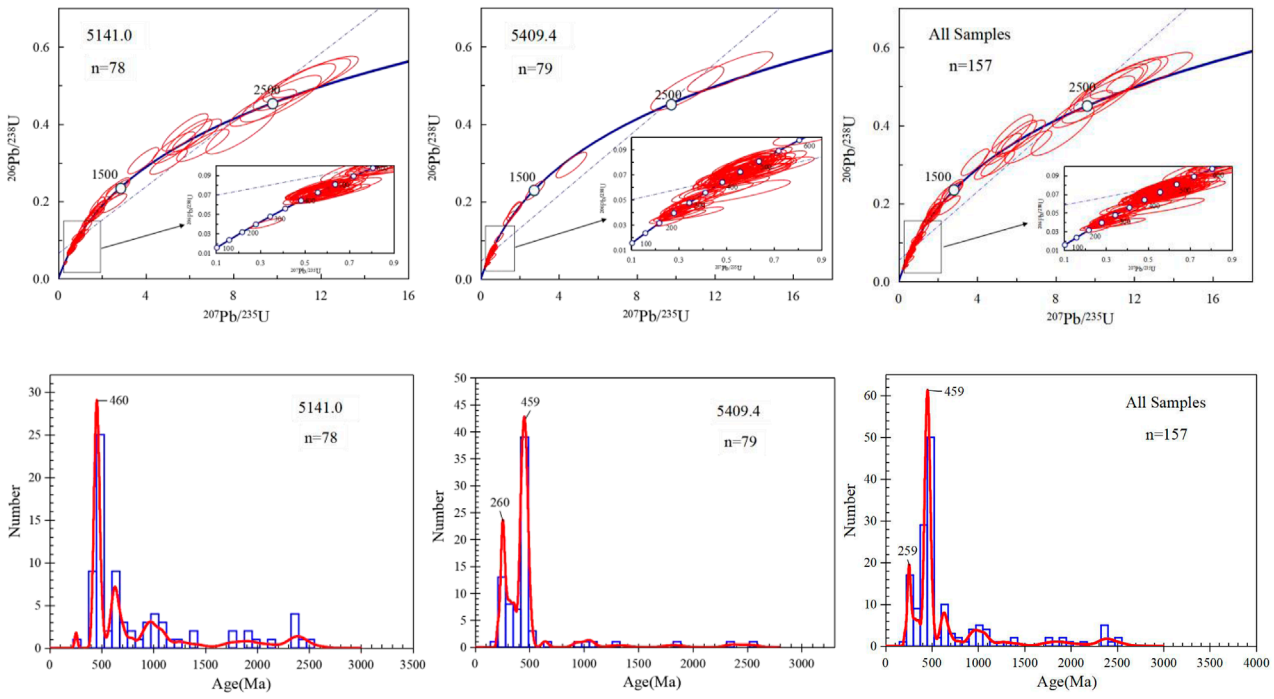

FIGURE 4
U-Pb concordia plots, histograms and normalized probability curves of ages of detrital zircons from sedimentary samples of the West Kunlun piedmont belt.

The Paleozoic and Mesozoic zircons are mainly concentrated in the age of detrital zircons, especially the two samples have their age peaks between 400 and 500 Ma, which is related to the Tethys evolution occurring in the Tarim Craton and its periphery from Sinian to Carboniferous. Since the subduction of the Proto-Tethys Ocean to the formation of the Neo-Tethys Ocean covers the whole Paleozoic to Mesozoic. During this period, magmatic hydrothermal activity occurred continuously in the southern margin of Tarim, the West Kunlun orogenic belt and its surrounding terranes, so it can be considered that the Paleozoic and Mesozoic detrital zircons in this experiment are derived from Tethian evolution. Two of the major peaks in the two age ranges of 300–200 Ma and 500–400 Ma have been found in these areas, such as the 430 Ma granite reported in the Tiekelik area (Ye et al., 2008). Biotite granite of 442 Ma reported in the eastern section of West Kunlun (Han, 2002), granodiorite of 215 Ma reported in the southern area of Kudi (Liu et al., 2015).

5.2 Provenance analysis

The main sources of detrital zircons in the sedimentary basin are the orogenic belts around the basin. The West Kunlun piedmont belt is located in the northern part of the Qinghai-Tibet Plateau. The main surrounding terranes are Qiangtang Terrane, East Kunlun orogenic belt, Songpan-Ganzi Terrane, Tianshuihai Terrane, North and South Kunlun Terranes and Tarim Basin. In order to accurately determine the provenance of Cretaceous sedimentary strata by zircon U-Pb age, a large number of Mesozoic and Paleozoic zircon age data were collected from Qiangtang Terrane, East Kunlun orogenic belt, Songpan-Ganzi Terrane, Tianshuihai Terrane, North and South Kunlun Terranes, Tarim Basin and other geological bodies (Figure 5). The U-Pb age data of plastids from different regions are drawn into zircon age spectrum. In addition, the granite age data reported by predecessors in West Kunlun area are summarized.

In the compiled age groups of granites from the West Kunlun region, it is evident that the ages are distinctly divided according to the regions. The granite age of the North and South Kunlun has two main intervals of 300–200 Ma and 500–400 Ma, which are not available in other terranes in the West Kunlun area (Figure 6). We speculate that the South and North Kunlun have great possibility to provide provenance for the piedmont belt. The comparison of detrital zircon age spectra from the peripheral terranes shows that the peak values of Songpan-Ganzi terrane mainly occur at 255 Ma, 439 Ma, 771 Ma and 1,860 Ma, although the peaks of 300–200 Ma and 500–400 Ma are similar to those of the Cretaceous samples. However, a large number of detrital zircons in the Songpan-Ganzi terrane at 800–700 Ma and 1,900–1,800 Ma are not found in the Cretaceous detrital zircons in the piedmont belt, so the Songpan-Ganzi terrane is not the main source of Cretaceous deposits in the piedmont belt. The age distribution of detrital zircons is similar between the East Kunlun orogenic belt and the North and South Kunlun terranes, and their peak ranges are both 300–200 Ma and 500–400 Ma, which are the reasonable source areas of the Cretaceous strata in the piedmont belt. Although the Qiangtang

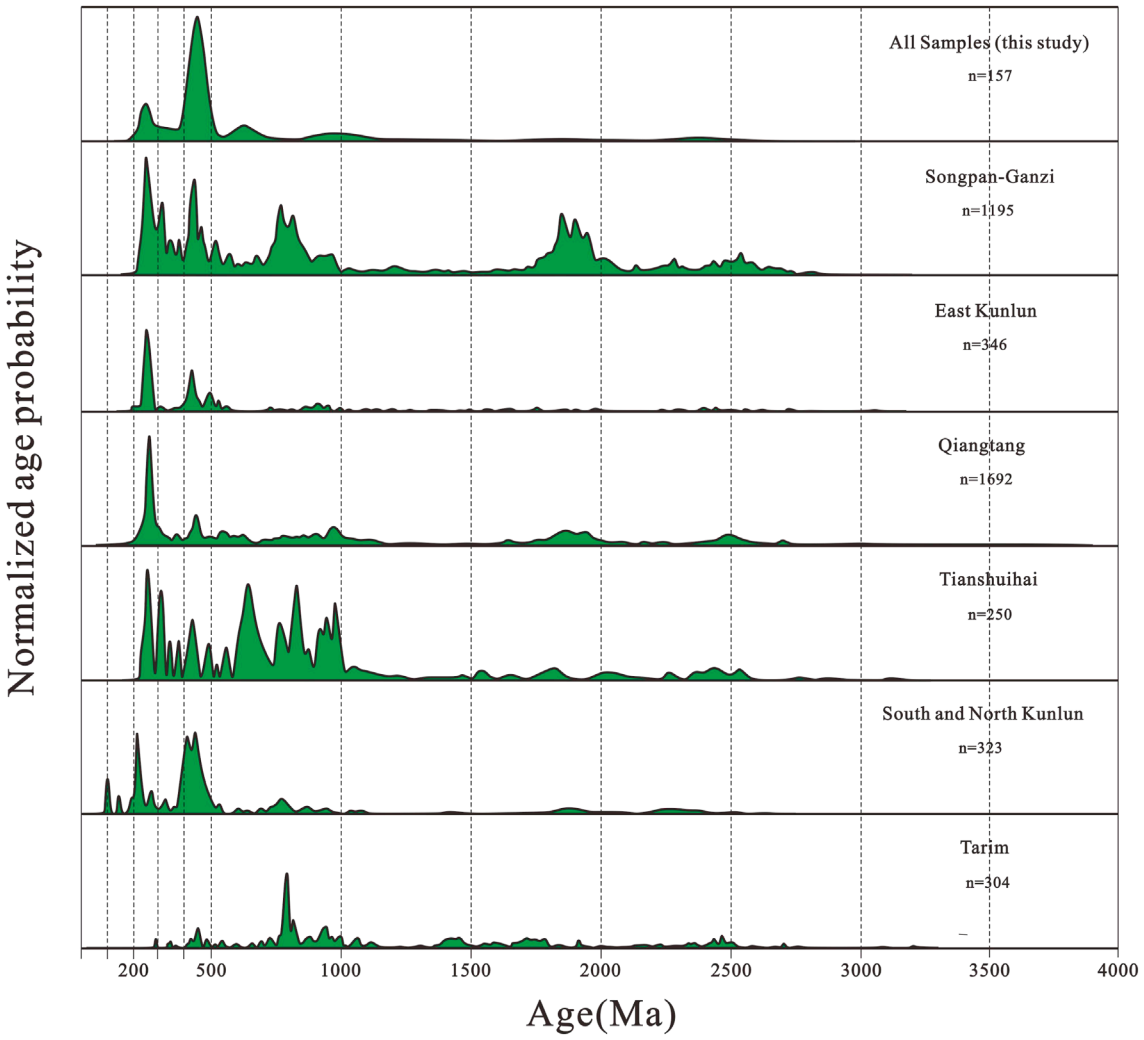

FIGURE 5
Age distribution of Cretaceous zircons in Piedmont and surrounding areas. Songpan-Ganzi (Ding et al., 2013); East Kunlun (Ding et al., 2013); Qiangtang (Gehrels et al., 2011; Ding et al., 2013); Tianshuihai (Hu et al., 2016; Dong et al., 2019); South and North Kunlun (Blayney et al., 2016); Tarim (Rojas-Agramonte et al., 2011).

terrane has an obvious peak value between 300 and 200 Ma, the peak value between 500 and 400 Ma is not obvious. While the Tianshuihai terrane has a peak value between 300 and 200 Ma and 500 and 400 Ma, there are a lot of zircons between 1,000 and 600 Ma, which is not available in the Cretaceous samples in the piedmont belt. Therefore, Qiangtang and Tianshuihai terranes are not the main sources of Cretaceous deposits in the piedmont zone. The age distribution of zircons in the Tarim Basin is very complex, and the peak value of zircons does not appear below 500 Ma, so the internal source of the Tarim Basin is very limited. It is speculated that the uplift of the West Kunlun orogenic belt has played a major role in controlling the deposition of the piedmont belt, so the provenance of the Tarim is less than that of the Tethys tectonic terrane. Based on the age distribution of granites and detrital zircons in different regions, it can be concluded that the North and South Kunlun terrane is the main source of Cretaceous in the piedmont belt, and the East Kunlun orogenic belt has the possibility of providing the source of the piedmont belt.

5.3 Implications for tectonic evolution in West Kunlun

The Qinghai-Tibet Plateau is a vast composite orogen that has undergone multiple orogenic events during the Early Paleozoic, Triassic, Late Mesozoic and Cenozoic periods (Tapponnier P et al., 1986; Molnar, 1988). The detrital zircons in the Cretaceous sediments of the West Kunlun piedmont belt are closely related to the dynamic environment and regional paleogeographic background of the terrane and the surrounding terrane. This includes the evolution of the Proto-Tethys Ocean starting in the Early Paleozoic, the subduction, reduction, and collision of the Paleo-Tethys Ocean beginning in the Late Paleozoic, and the associated orogenic processes (Li et al., 2018; Zhao et al., 2018). In recent years, the West Kunlun orogenic belt has been relatively poorly studied, and some key geological questions remain unanswered, including its orogenic processes. In recent years, new evidence has been continuously speculated. For example, Jiang, (1992) summarized

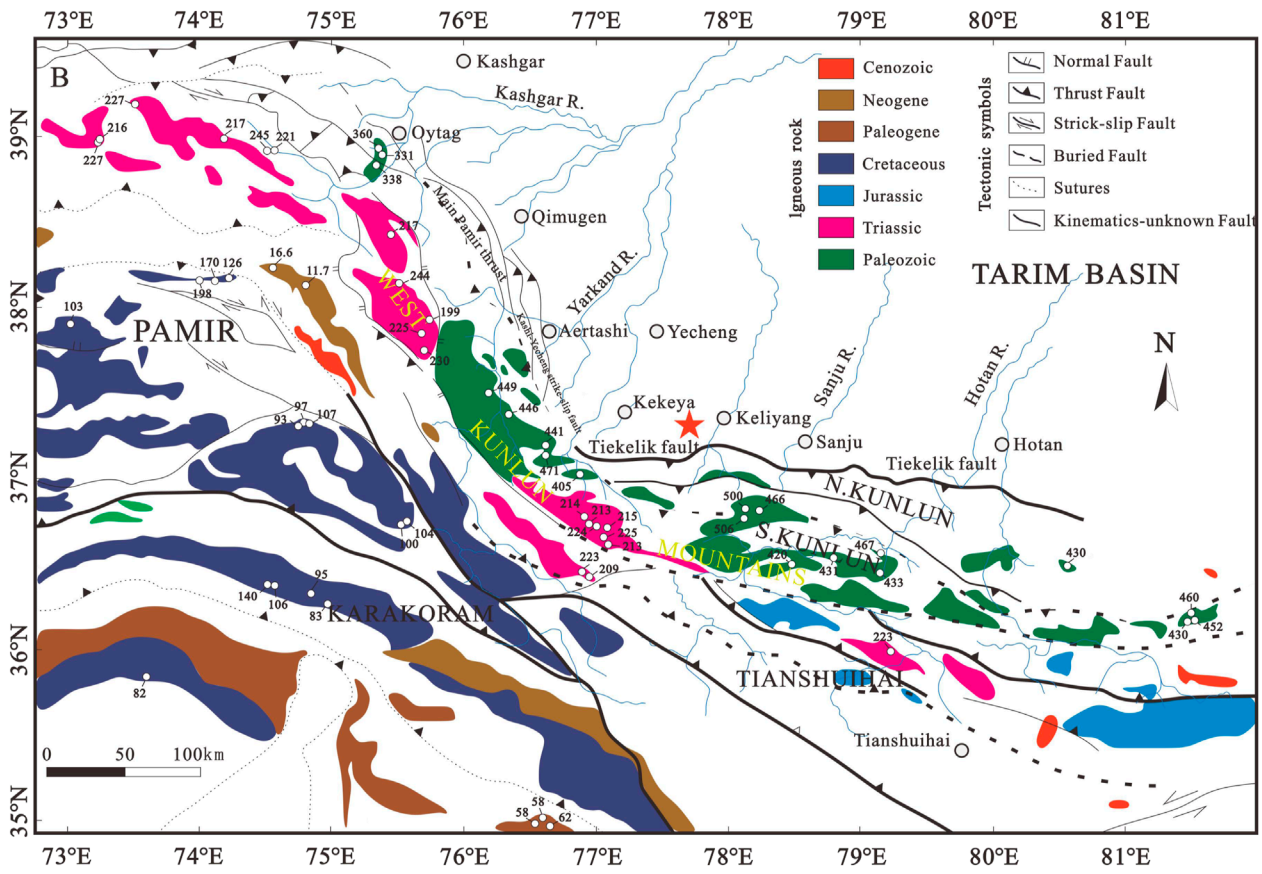

FIGURE 6
Igneous rock distribution with U-Pb ages within the West Kunlun and the adjacent areas.

the regional tectonic evolution of West Kunlun as two splits, two collisions and one overlay based on the view of open-close structures, that is, the West Kunlun orogenic belt experienced two ocean-forming fractures, two subduction collisions and one overlay orogenic process (land-continental subduction orogenic process) (Jiang, 1992). Wang, (2004) believed that the collision of North Kunlun terrane and South Kunlun terrane occurred in the Devonian period, and then the subduction of the Paleo-Tethys Ocean to the north began again, resulting in the formation of the Carboniferous Jurassic magmatic arc. The Paleo-Tethys Ocean finally closed in the Late Triassic to Early Jurassic period, resulting in the collision between the Karakoram-Qiangtang terranes and the southern margin of the South Kunlun terrane, forming the early West Kunlun orogenic belt (Wang, 2004). Han, (2006) proposed the multi-island ocean-continuous accretion model, suggesting that the West Kunlun orogenic belt is a complex accretionary orogen with long-term evolution, and the Qinqi-Kun ocean slab, formed during the Sinian-Cambrian expansion, continuously subducted beneath the northern side of the Tarim Craton from the Ordovician to the Triassic, leading to the southward accretion of the Tarim Craton (Han, 2006). According to the above conditions, the time of cracking and closing of the Proto-Paleo-Tethys ocean is the key to the formation of the West Kunlun orogenic belt.

The age distribution of 108 zircons smaller than 600 Ma can be divided into three groups: 520–407 Ma, 385–310 Ma, and 290–200 Ma (Figure 7). In the late Early Paleozoic, the southern Tarim Craton was closed, forming the West Kunlun Early Paleozoic collision orogenic belt, which also represents the closure of the Proto-Tethys Ocean. According to the geochemical characteristics of Early Paleozoic granite published by predecessors, 500–450 Ma granite has typical I-Type characteristics, and the data of this time produced a peak value around 450 Ma, and an obvious fall after 450 Ma. We hypothesized that the subduction of the Proto-Tethys oceanic crust occurred before 500 Ma and continued until 450 Ma, and that 450 Ma is the time when the subduction of the Proto-Tethys oceanic crust subducted until the collision between the plates began. A large number of 430–400 Ma granites evolved from high Ba-Sr to A-type granites discovered by predecessors in the West Kunlun area (Yuan, 1999; Yuan et al., 2002; Ye et al., 2008), at the same time, 420 to 405 Ma A-type granite was found in the reservoir area, and it was proved that it was exposed to the intraplate extension environment (Wang et al., 2020). Combined with the zircon in this experiment, it appeared to fall after 450 Ma. We speculate that the South Kunlun terrane and the North Kunlun terrane completed the convergence between 430 and 420 Ma, and this closure also represents the closure of the original Tethys Ocean, and the entire collision orogeny lasted to about 400 Ma.

At the end of the Early Permian, the Paleo-Tethys Ocean subducted northward, leading to the collision of the Qiangtang

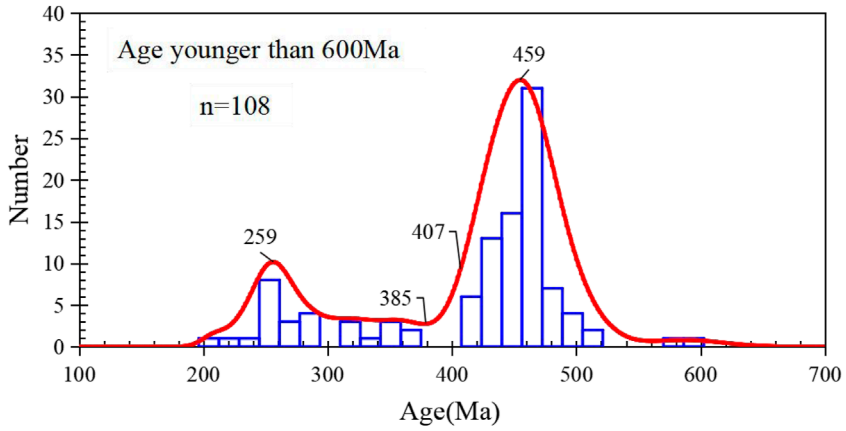

FIGURE 7
All samples detrital zircon age (younger than 600 Ma).

Terrane with the Tarim Craton. Previous studies suggest that from 338 Ma to 251 Ma, the Paleo-Tethys Ocean underwent northward subduction. The South Kunlun Terrane and the Tianshuihai Terrane collided around 243 Ma and completed suturing by 228 Ma, marking the final closure of the Paleo-Tethys Ocean (Jiang et al., 2013), and the Kangxiwar ophiolite belt is the product of the closure of this collision, and the southwest Tarim developed into a back-arc foreland basin. In this experiment, the peak value showed a groove shape between 400 and 300 Ma, and there were gaps between 400–380 Ma and 310–290 Ma, and there are two distinct processes of peaks rising and falling. Therefore, we think that the two openings and two collisions of the West Kunlun orogenic belt are reasonable, and there is a certain vacancy between the two openings, which also indicates that the continuity between the Proto-Tethys Ocean and the Paleo-Tethys Ocean is not obvious, and there may be a long interval. The piedmont belt and the surrounding terranes, excluding the Tarim Basin, all exhibit peak values around 250 Ma. This indicates that the subduction of the Paleo-Tethys Ocean crust affected these terranes, with both the internal terranes of the Western Kunlun and the surrounding micro-terranes participating in the cyclical evolution of the Paleo-Tethys Ocean. Due to the absence of Triassic deposits in the Southwest Tarim Depression, there is a great debate on tectonic evolution. Some people believe that the West Kunlun orogenic belt and the South Tianshan Mountains are still in the process of orogeny, and the West Kunlun orogenic belt developed thrust-fault structures in front of them (Wu, 2018). Others believe that the orogenic belt was completely formed in the Triassic. Then it enters the stage of in-plate activity completely (Fang et al., 2009; Cheng et al., 2019), combined with the age distribution of about 290–200 Ma in this experiment and the age of the youngest single-grain zircon 208 Ma, we believe that during the early 250 Ma of the Triassic, the evolution of the Paleo-Tethys Ocean changed from oceanic subduction stage to continental collision. The intercontinental collision that lasted throughout the Triassic prevented the piedmont zone from receiving Triassic deposits. However, the Cretaceous period where this sample is located is more than 50 Ma different from the Triassic period, and there is no relevant age during this period, indicating that there is a lack of effective volcanic activity records in the West Kunlun region after the Triassic period, and all the peripheral plates were collaged at the end of the Triassic period. No matter what the explanation is, the Triassic period is a transition period of tectonic evolution into an introntinental evolution stage. In general, the timing of the Paleo-Tethys tectonic movement at the beginning of the Permian corresponds well to the main peak interval of 290–200 Ma in this study.

6 Conclusion

(1) The Cretaceous detrital zircons in the piedmont belt are aged 290-208 Ma, 520–310 Ma, 810–580 Ma, 1,400–880 Ma, and 2,548–1730 Ma, indicating that the provenance in this area is very complex.

(2) By comparing the ages of granites and detrital zircons from different peripheral terranes, it is suggested that the Cretaceous strata in the piedmont belt originated from the North and South Kunlun terranes, and may also come from the East Kunlun orogenic belt. The formation of the whole West Kunlun orogenic belt experienced two opening and two closing processes. The microlandmasses in and around the West Kunlun orogenic belt are involved in the evolution of the Proto-Tethys Ocean and the Paleo-Tethys Ocean.

(3) The subduction of the Proto-Tethys Ocean occurred before 500 Ma and lasted until 450 Ma. 450 Ma is the time when the subduction of the Proto-Tethys Ocean subducted to the collision between the plates. The suturing between the South Kunlun Terrane and the North Kunlun Terrane was completed in 430–420 Ma, which also represents the closure of the Proto-Tethys Ocean. The entire Proto-Tethys collision orogeny lasted until about 400 Ma. All microlandmasses in the West Kunlun orogenic belt were collaged during the Triassic period, and there is no record of effective volcanic activity between the Triassic and Cretaceous.

(4) The subduction of the Paleo-Tethys Ocean occurred before 290 Ma, and transformed from the subduction phase to

continental collision before 250 Ma. All the microlandmasses were completely collaged at the end of the Triassic, corresponding to the end of the evolution of the ancient TethysJ Ocean, and the tectonic evolution completely entered the stage of intracontinental evolution.

Data availability statement

The original contributions presented in the study are included in the article/Supplementary Material, further inquiries can be directed to the corresponding author.

Author contributions

YG: Conceptualization, Data curation, Investigation, Methodology, Writing–original draft. LJ: Funding acquisition, Investigation, Project administration, Writing–review and editing. WC: Conceptualization, Methodology, Writing–review and editing. FJ: Conceptualization, Supervision, Writing–review and editing. HD: Project administration, Supervision, Writing–review and editing. WZ: Writing–review and editing. CD: Data curation, Writing–review and editing. YF: Investigation, Writing–review and editing.

Funding

The author(s) declare that financial support was received for the research, authorship, and/or publication of this article. This work was supported by the Second Tibetan Plateau Scientific Expedition and Research Program (STEP), Grant No. 2019 QZKK0708, and the National Natural Science Foundation of China, Grant No. U22B6002.

Conflict of interest

YG, LJ, WC, HD, and WZ were employed by the PetroChina.

The remaining authors declare that the research was conducted in the absence of any commercial or financial relationships that could be construed as a potential conflict of interest.

Publisher's note

References

Blayney, T., Najman, Y., Dupont-Nivet, G., Carter, A., Millar, I., Garzanti, E., et al. (2016). Indentation of the Pamirs with respect to the northern margin of Tibet: constraints from the Tarim basin sedimentary record. *Tectonics* 35 (9-10), 2345–2369. doi:10.1002/2016tc004222

Cao, K., Wang, G., Bernet, M., van der Beek, P., and Zhang, K. (2015). Exhumation history of the West Kunlun Mountains, northwestern Tibet: evidence for a long-lived, rejuvenated orogen. *Earth Planet. Sci. Lett.* 432, 391–403. doi:10.1016/j.epsl.2015.10.033

Cawood, P. A., Hawkesworth, C. J., and Dhuime, B. (2012). Detrital zircon record and tectonic Setting. *Geology* 40 (10), 875–878. doi:10.1130/g32945.1

Chen, H. L., Li, K., Li, Y., Wu, H. X., Cheng, X. G., Zeng, C. M., et al. (2018). The segmentation deformation of the thrust belt in front of Western Kunlun, western China, and its controlling factors. *Acta Petrol. Sin.* 34 (7), 1933–1942. in Chinese with English abstract.

Cheng, X. G., Wu, H. X., Li, Y., Chen, H. L., Zhang, F. Q., and Shi, J. (2019). Influences of indosinian structures on later structural deformation and sedimentation in piedmont of western Kunlun Mountains. *Xinjiang Pet. Geol.* 40 (01), 27–33. in Chinese with English abstract. doi:10.7657/XJPG20190104

Ding, L., Yang, D., Cai, F. L., Pullen, P., Zhang, L. Y., Zhang, Q. H., et al. (2013). Provenance analysis of the Mesozoic Hoh-Xil-SongpanGanzi turbidites in northern Tibet: implications for the tectonic evolution of the eastern Paleo-Tethys Ocean. *Tectonics* 32, 34–48. doi:10.1002/tect.20013

Dong, R., Wang, H., Yan, Q. H., Zhang, X. Y., Wei, X. P., Li, P., et al. (2019). Geochemical characteristics and zircon U-Pb ages of the bayankalashan group in the tianshihai terrain of the West Kunlun orogenic belt: implication for its provenance and tectonic environment. *Geotect. Metallogenia* 43 (6), 1236–1257. doi:10.16539/j.ddgzyckx.2019.06.011

Fang, A. M., Ma, J. Y., Wang, S. G., Zhao, Y., and Hu, J. M. (2009). Sedimentary tectonic evolution of the southwestern Tarim Basin and west Kunlun orogen since late paleozoic. *Acta Petrol. Sin.* 25 (12), 3396–3406. in Chinese with English abstract.

Ge, R., Wilde, S. A., Zhu, W., Zhou, T., and Si, Y. (2022). Formation and evolution of archean continental crust: a thermodynamic - geochemical perspective of granitoids from the Tarim Craton, NW China. *Earth-Science Rev.* 234, 104219. doi:10.1016/j.earscirev.2022.104219

Gehrels, G., Kapp, P., Decelles, P., Pullen, A., Blakey, R., Weislogel, A., et al. (2011). Detrital zircon geochronology of pre-Tertiary strata in the Tibetan-Himalayan orogen. *Tectonics* 30 (5), TC5016.1–TC5016.27. doi:10.1029/2011tc002868

Guo, X. C., Zheng, Y. Z., Gao, J., and Zhu, Z. X. (2013). Determination and geological significance of the mesoarchean Craton in western Kunlun Mountains. *Xinjiang,China. Geol. Rev.* 59 (03), 401–412. in Chinese with English abstract. doi:10.16509/j.georeview.2013.03.015

Han, F. L. (2002). *Qimanyuter ophiolite melange and its tectonic Significance,Western Kunlun mountain,NW China*. Beijing: China University of Geosciences. in Chinese with English abstract.

Han, F. L. (2006). *Tectonic evolution and mineralizationof the western Kunlun accretion-type orogen*. Beijing: China University of Geosciences. in Chinese with English abstract.

Hoskin, P. W. O., and Schaltegger, U. (2003). The composition of zircon and igneous and metamorphic petrogenesis. *Rev. mineralogy Geochem.* 53 (1), 27–62. doi:10.2113/0530027

Hu, J., Wang, H., Huang, C. Y., Tong, L. X., Mu, S. L., and Qiu, Z. W. (2016). Geological characteristics and age of the Dahongliutan Fe-ore deposit in the Western Kunlun orogenic belt, Xinjiang, northwestern China. *J. Asian Earth Sci.* 116, 1–25. doi:10.1016/j.jseaes.2015.08.014

Jiang, C. F. (1992). *Kunlun opening and closing structure*. Chinese.

Jiang, L., Dong, H. K., Li, Y., Zhao, W., Zhang, Y. Q., and Bo, D. M. (2024). Deformation characteristics and exploration potential of the West Kunlun foreland fold-and-thrust belt. *Adv. Geo-Energy Res.* 11 (3), 181–193. doi:10.46690/ager.2024.03.03

Jiang, Y. H., Jia, R. Y., Liu, Z., Liao, S. Y., Zhao, P., and Zhou, Q. (2013). Origin of Middle Triassic high-K calc-alkaline granitoids and their potassic microgranular enclaves from the western Kunlun orogen, northwest China: a record of the closure of Paleo-Tethys. *Lithos* 156-159, 13–30. doi:10.1016/j.lithos.2012.10.004

John, B., Carmala, N. G., Lindsay, S., George, G., and Li, T. (2012). Cenozoic evolution of the Pamir plateau based on stratigraphy, zircon provenance, and stable isotopes of foreland basin sediments at Oytag (Wuyitake) in the Tarim Basin (west China). *J. Asian Earth Sci.* 44, 136–148. doi:10.1016/j.jseaes.2011.04.020

Li, C. M. (2009). A review on the minerageny and situ microanalytical DatingTechniques of zircons. *Geol. Survery Res.* 32 (3), 161–174. in Chinese with English abstract.

Li, S. Z., Zhao, S., Liu, X., Cao, H. H., Yu, S., Li, X. Y., et al. (2018). Closure of the Proto-Tethys Ocean and early paleozoic amalgamation of microcontinental blocks in east asia. *Earth-Science Rev.* 186, 37–75. doi:10.1016/j.earscirev.2017.01.011

Liu, Z., Jiang, Y. H., Jia, R. Y., Zhao, P., and Zhou, Q. (2015). Origin of Late Triassic high-K calc-alkaline granitoids and their potassic microgranular enclaves from

the western Tibet Plateau, northwest China: implications for Paleo-Tethys evolution. *Gondwana Res.* 27, 326–341. doi:10.1016/j.gr.2013.09.022

Long, X. P., Yuan, C., Sun, M., Alfred, K., Zhao, G. C., Simon, W., et al. (2011). Reworking of the Tarim Craton by underplating of mantle plume-derived magmas: evidence from Neoproterozoic granitoids in the Kuluketage area, NW China. *Precambrian Res.* 187 (1–2), 1–14. doi:10.1016/j.precamres.2011.02.001

Molnar, P. (1988). A review of geophysical constrains on the deep structure of the Tibetan Plateau, the Himalaya and the Karakoram, and their tectonic implications. *Phil. Trans. R. Soc. Lond* A326, 33–88.

Rojas-Agramonte, Y., Kröner, A., Demoux, A., Xia, X., Wang, W., Donskaya, T., et al. (2011). Detrital and xenocrystic zircon ages from Neoproterozoic to Palaeozoic arc terranes of Mongolia: significance for the origin of crustal fragments in the Central Asian Orogenic Belt. *Gondwana Res.* 19, 751–763. doi:10.1016/j.gr.2010.10.004

Shu, L. S., Deng, X. L., Zhu, W. B., and Xiao, W. (2011). Precambrian tectonic evolution of the Tarim Block, NW China: new geochronological insights from the Quruqtagh domain. *J. Asian Earth Sci.* 42 (5), 774–790. doi:10.1016/j.jseaes.2010.08.018

Tapponnier, P., Peltzer, G., and Armijo, R. (1986). "On the mechanics of the collision between Indian and Asia," in *Collision tectonics*. Editors M. P. Coward, and A. C. Ries (Geological Journal), 19, 115–157.

Wang, C., Liu, L., Wang, Y. H., He, S. P., Li, R. S., Li, M., et al. (2015). Recognition and tectonic implications of an extensive Neoproterozoic volcano-sedimentary rift basin along the southwestern margin of the Tarim Craton, northwestern China. *Precambr. Res.* 257, 65–82. doi:10.1016/j.precamres.2014.11.022

Wang, P., Zhao, G. C., Han, Y. G., Liu, Q., Yao, J. L., Yu, S., et al. (2020). Timing of the final closure of the Proto-Tethys Ocean: constraints from provenance of early paleozoic sedimentary rocks in West Kunlun, NW China. *Gondwana Res.* 84, 151–162. doi:10.1016/j.gr.2020.04.001

Wang, Z. H. (2004). Tectonic evolution of the western Kunlun orogenic belt, western China. *J. Asian Earth Sci.* 24, 153–161. doi:10.1016/j.jseaes.2003.10.007

Wu, H. X. (2018). *Characteristics of paleostructure in the mountain front region ofsouthwestern Tarim Basin and its control of Jurassic-Cretaceousdeposition*. Zhejiang University. in Chinese with English abstract.

Wu, H. X., Cheng, X. G., Chen, H. L., Chen, C., Dilek, Y., Shi, J., et al. (2021). Tectonic switch from triassic contraction to jurassic-cretaceous extension in the western Tarim Basin, northwest China: new insights into the evolution of the paleo-tethyan orogenic belt. *Front. Earth Sci.* 9, 636383. doi:10.3389/feart.2021.636383

Wu, Y. B., and Zheng, Y. F. (2004). Genetic mineralogy of zircon and its restriction on U-Pb age interpretation. *Chin. Sci. Bull.* 49 (16), 1589–1604. in Chinese.

Xin, H. T., Zhao, F. Q., Luo, Z. H., Liu, Y. S., Wan, Y. S., and Wang, S. Q. (2011). Determination of the paleoproterozoic geochronological framework in aqtashtagh area in southeastern Tarim,China,and its geological significance. *Acta Geol. Sin.* 85 (12), 1977–1993. in Chinese with English abstract. doi:10.1007/s11629-011-2067-x

Xu, B., Xiao, S. H., Zou, H. B., Chen, Y., Li, Z. X., Song, B., et al. (2009). SHRIMP zircon U-Pb age constraints on Neoproterozoic Quruqtagh diamictites in NW China. *Precambrian Res.* 168 (3-4), 247–258. doi:10.1016/j.precamres.2008.10.008

Yang, W. Q., Liu, L., Cao, Y. T., Wang, C., He, S. P., Li, R. S., et al. (2010). Geochronological evidence of Indosinian (high-pressure) metamorphic event and its tectonic significance in Taxkorgan area of the Western Kunlun Mountains, NW China. *Sci. China Earth Sci.* 53 (10), 1445–1459. doi:10.1007/s11430-010-4081-1

Ye, H. M., Li, X. H., Li, Z. X., and Zhang, C. L. (2008). Age and origin of high Ba–Sr appinite–granites at the northwestern margin of the Tibet Plateau: implications for early Paleozoic tectonic evolution of the Western Kunlun orogenic belt. *Gondwana Res.* 13 (1), 126–138. doi:10.1016/j.gr.2007.08.005

Yin, J. Y., Xiao, W. J., Sun, M., Chen, W., Yuan, C., Zhang, Y. Y., et al. (2020). Petrogenesis of early cambrian granitoids in the western Kunlun orogenic belt, northwest tibet: insight into early stage subduction of the Proto-Tethys Ocean. *Geol. Soc. Am. Bull.* 132 (9-10), 2221–2240. doi:10.1130/b35408.1

Yuan, C. (1999). *Magmatism and tectonic evolution of the West Kunlun Mountains (PhD dissertation)*. University of Hongkong.

Yuan, C., Sun, M., Zhou, M. F., Zhou, H., Xiao, W. J., and Li, J. L. (2002). Tectonic evolution of the West Kunlun: geochronologic and geochemical constraints from Kudi granitoids. *Int. Geol. Rev.* 44, 653–669. doi:10.2747/0020-6814.44.7.653

Zhang, C. L., Dong, Y. G., Zhao, Y., Wang, A. G., and Guo, K. Y. (2003). Geochemistry of mesoproterozoic volcanic rocks in the western Kunlun mountains:evidence for plate tectonic evolution. *Acta Geol. Sin. -English Ed.* 77 (2), 237–245. doi:10.1111/j.1755-6724.2003.tb00567.x

Zhang, C. L., Li, Z. X., Li, X. H., and Ye, H. M. (2007). An early Paleoproterozoic high-K intrusive complex in southwestern Tarim Block, NW China: age, geochemistry, and tectonic implications. *Gondwana Res.* 12, 101–112. doi:10.1016/j.gr.2006.10.006

Zhang, C. L., Yang, D. S., Wang, H. Y., Yutaka, T., and Ye, H. M. (2011). Neoproterozoic mafic-ultramafic layered intrusion in Quruqtagh of northeastern Tarim Block, NW China: two phases of mafic igneous activity with different mantle sources. *Gondwana Res.* 19 (1), 177–190. doi:10.1016/j.gr.2010.03.012

Zhang, C. L., Ye, H. M., Wang, A. G., Guo, K. Y., and Dong, Y. G. (2004). Geochemistry of the Neoproterozoic diabase and basalt in the south of Tarim plate: evidence for the Neoproterozoic breakup of the Rodinia supercontinent in the south of Tarim. *Acta Petrol. Sin.* 20, 473–482. (in Chinese with English abstract). doi:10.3321/j.issn:1000-0569.2004.03.011

Zhang, C. L., Yu, H. F., Wang, A. G., and Guo, K. Y. (2005). Dating of triassic granites in the western Kunlun Mountains and its tectonic significace. *Acta Geol. Sin.* 05, 645–652. (in Chinese with English abstract).

Zhang, C. L., Zou, H. B., Li, H. K., and Wang, H. Y. (2013). Tectonic framework and evolution of the Tarim block in NW China. *Gondwana Res.* 23 (4), 1306–1315. doi:10.1016/j.gr.2012.05.009

Zhang, L., Long, X. P., Zhang, R., Dong, Y. P., Yuan, C., Xiao, W. J., et al. (2017). Source characteristics and provenance of metasedimentaryrocks from the kangxiwa group in the western Kunlun orogenic belt,NW China: implications for tectonic setting and crustal growth. *Gondwana Res.* 46, 43–56. doi:10.1016/j.gr.2017.02.014

Zhang, Y., Niu, Y., Hu, Y., Liu, J. J., Ye, L., Kong, J. J., et al. (2016). The syncollisional granitoid magmatism and continental crust growth in the West Kunlun Orogen, China – evidence from geochronology and geochemistry of the Arkarz pluton. *Lithos* 245, 191–204. doi:10.1016/j.lithos.2015.05.007

Zhang, Y. Z., Lin, C. S., Gao, Z. Y., Lu, G., Ren, Y. Z., Song, N. N., et al. (2014). Depositional paleogeography and provenance analysis of early cretaceous southwest depression of Tarim Basin. *Geoscience* 28 (04), 791–798. (in Chinese with English abstract).

Zhao, G. C., Wang, Y. J., Huang, B. C., Dong, Y. P., Li, S. Z., Zhang, G. W., et al. (2018). Geological reconstructions of the East asian blocks: from the breakup of Rodinia to the assembly of pangea. *Earth-Science Rev.* 186, 262–286. doi:10.1016/j.earscirev.2018.10.003

Zhu, D. C., Zhao, Z. D., Niu, Y. L., Dilek, Y., and Mo, X. X. (2011). Lhasa terrane in southern Tibet came from Australia. *Geology* 39 (8), 727–730. doi:10.1130/g31895.1

Zhu, W., Zhang, Z., Shu, L., Lu, H., Su, J., and Yang, W. (2008). SHRIMP U–Pb zircon geochronology of Neoproterozoic Korla mafic dykes in the northern Tarim Block, NW China: implications for the long-lasting breakup process of Rodinia. *J. Geol. Soc.* 165, 887–890. doi:10.1144/0016-76492007-174